CRANFIELD UNIVERSITY

JOANNA COOKNEY

METHANE MANAGEMENT IN SEWAGE TREATMENT

SCHOOL OF APPLIED SCIENCES

MSc
Academic Year: 2009 - 2011

Supervisor: Dr. Bruce Jefferson
July 2011

CRANFIELD UNIVERSITY

SCHOOL OF APPLIED SCIENCES

MSc

Academic Year 2009 - 2011

JOANNA COOKNEY

Methane management in sewage treatment

Supervisor: Dr. Bruce Jefferson

July 2011

Abstract

Poly-di-methyl-siloxane (PDMS) hollow fibre membrane modules were designed and built for the specific de-gassing of real and synthetic process liquids to understand: (i) the feasibility of operation; and (ii) classify the mass transfer characteristics to aid design at full scale. Liquid saturated with pure methane or a binary methane and carbon dioxide mixture was introduced into the shell side of the extraction unit, whilst sweep gas or vacuum was employed counter-currently as a stripping medium. From data analysis of operation in both anaerobic effluents obtained from Expanded Granular Sludge Blanket (EGSB) reactor and synthetic liquids, when operating under optimum conditions 93% of methane and 88% of carbon dioxide was recovered. The obtained data indicate that the extraction process is controlled by diffusivity of gases through the PDMS membrane and is proportional to the thickness of membrane wall. When applying vacuum to promote methane mass transfer, the process was highly sensitive to vacuum pressure; the highest de-gassing efficiency was recorded under the lowest absolute vacuum pressure. However, when vacuum was replaced by sweep gas, the process was insensitive to changes in gas velocity. When utilising PDMS membrane contactor for de-gassing of EGSB effluent, the net electrical output achieved by the EGSB increased by *c.* 24% and indicates that by integrating methane recovery, treatment of domestic wastewater using low temperature EGSB processes can become carbon positive. The potential of directing recovered methane to porous hollow fibre membrane absorbers and upgrading to national gas (NG) standards to use in national gas grid or as a vehicle fuel has been demonstrated.

Keywords:

Methane recovery; poly-di-methyl-siloxane; biogas; anaerobic   effluent; hollow fibre membrane contactors; methane management, carbon dioxide.

Acknowledgments

Table of Contents

List of Figures

List of Tables

List of Abbreviations

AMP	2-amino-2-methyl-1-propanol
BOD	biological oxygen demand
CEP	critical entry pressure
CHP	combined hate and power
COD	chemical oxygen demand
DEA	diethanolamine
DMEA	dimethylethanolamine
EGSB	Expanded Granular Sludge Blanket
GWP	global warming potential
HFMC	hollow fibre membrane contactor
HRT	hydraulic retention time
HS-GC	headspace gas chromatography
IR	poly-iso-propene
MDEA	methyl-di-ethanol-amine
NG	natural gas
NIPS	non-solvent induced phase inversion
PAMAM	polyamidoamine
PC	polycarbonate
PDMS	poly-di-metyl-siloxane
PE-HD	high-density polyethylelene
PI	polyimide
PP	polypropylene
PPhMS	poly-phenyl-methyl-siloxane
PPMS	poly-propyl-methyl-siloxane
PSA	Pressure Swing Adsorption
PTFE	polytetrafluoroethylene
PTFPMS	poly-tri-fluoro-propyl-methyl-siloxane
PVC	poly-vinyl-chloride
PVDF	polyvinyldieneflupride
PZ	piperazine
SEM	scanning electron microscopy
STP	standard temperature and pressure
TEA	triethanolamine
TSS	total suspended solids

Nomenclature

General

a, b, c	constant	-
A	membrane contact area	m^2
C	concentration	$mol.m^{-3}$ or $mg.L^{-1}$
d	diameter	m
D	diffusivity	$m^2.s^{-1}$
E	enhancement factor for chemical reaction	-
H	distribution coefficient	-
J	molar flux	$mol.s^{-1}$
k	individual mass transfer coefficient	$m.s^{-1}$
k_L^0	physical mass transfer coefficient	s^{-1}
K	overall mass transfer coefficient	$m.s^{-1}$
m	partitioning coefficient of the compound between membrane and the liquid phase	-
M	mass	mg or kg
P	permeability	Barrers
P_{VAC}	pressure	kPa or mBar
Q	flow rate	$m^3.s^{-1}$
r	hollow fibre radius	m
R	mass transfer resistance	$s.m^{-1}$
S	solubility	$cm^3STP.cm^{-3}.cmHg^{-1}$
Sc	Schmidt number	-
Sh	Sherwood number	-
V	velocity	$m.s^{-1}$
Vol	volume	mL
X	gas concentration at equilibrium between gas and liquid phase	$mg.mL^{-1}$

Greek symbols

α	Bunsen solubility coefficient	-
γ	surface tension	$mN.m^{-1}$
$\varDelta$	difference	
θ	contact angle between the solid surface and the liquid	°
μ	fluid viscosity	Pa.s
ρ	fluid density	$kg.m^{-3}$

Subscripts

CH_4	methane
CO_2	carbon dioxide
E	empty
F	filled
G	gas
h	hydraulic

i	inner
in	inlet
lm	logarithmic mean
L	liquid
M	membrane
o	outer
out	outlet
OV	overall
p	pore
V	vial
VAC	vacuum

Superscripts

P	permeate
*	at equilibrium

1 Introduction

1.1 General

Conventional wastewater treatment consists of preliminary removal of large objects and grit followed by sedimentation and biological treatment in the form of either suspended growth (activated sludge) or biofilm (trickling filters) processes (Figure 1). Captured solids are then further processed anaerobically to reduce solids volumes prior to final disposal including the production of biogas as a by product of the anaerobic reaction.
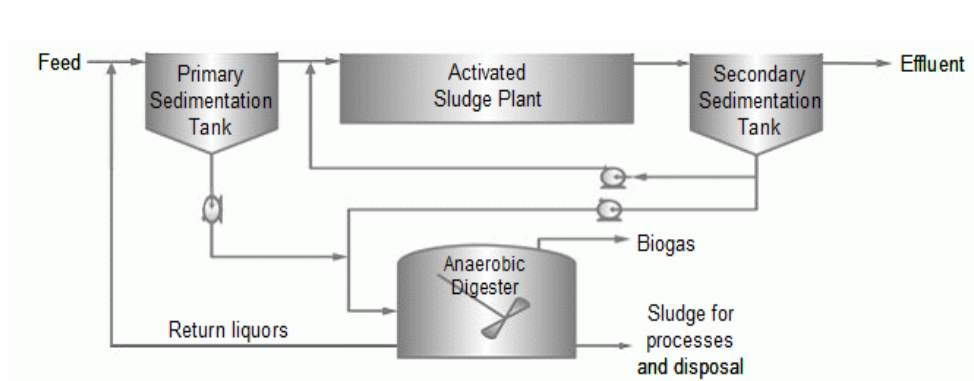
Figure 1. Conventional wastewater treatment plant.

To date, the activated sludge process has remained a core technology for the effective treatment of low temperature domestic wastewater in the UK, however, the energy demanded for aeration within the ASP comprises *c.* 55% of the electrical demand for wastewater treatment (*Tchobanoglous et al., 2003*). Therefore, several research groups have proposed anaerobic treatment as a substitute technology for ASP (Figure 2) as these conditions facilitate the reduction of organic carbon in the absence of air (*McAdam et al., 2010; Uemura and Harada, 2000*) and have the potential to reduce the energy demand of the total wastewater flowsheet by up to 62.5% (*McAdam et al., 2010*).
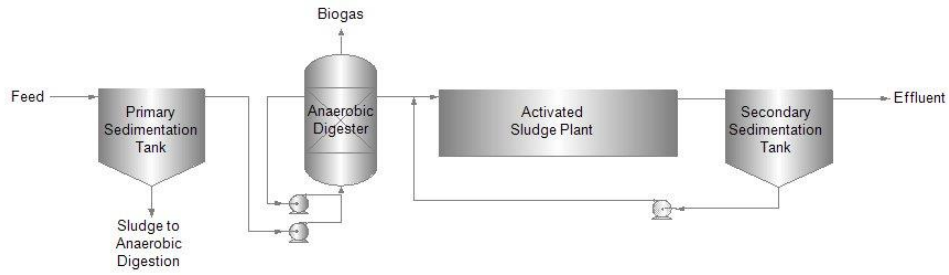
Figure 2. Wastewater treatment plant with integrated anaerobic digester

.

The composition of generated biogas depends on the source of the digested substrate, and typically consist 50-70 vol.% of methane (CH_4) and 20-50 vol.% of carbon dioxide (CO_2). In addition, nitrogen (N_2), hydrogen sulphide (H_2S), oxygen (O_2), ammonia (NH_3) and water vapour are present in small amounts (Table 1). However, when treating low-strength domestic wastewater, methane content in the off-gas rises to 70-80 vol.% in balance with 5-10 vol.% of CO_2 and 10-25 vol.% of N_2 (*Noyola et al., 1988*).

Table 1. Typical biogas composition from different sources of biodegradable matter.

Component	Unit	Household waste	Wastewater treatment	Agricultural waste	Food industry
CH_4	vol.%	50-60	60-75	60-75	68
CO_2	vol.%	34-38	19-33	19-33	26
N_2	vol.%	0-5	0-1	0-1	-
O_2	vol.%	0-1	< 0.5	< 0.5	-
H_2O	vol.%	5-6	5-6	5-6	5-6
H_2S	mg.m^{-3}	100-900	1000-4000	3000-10000	400
NH_3	mg.m^{-3}	-	-	50-100	-
Other trace gases	mg.m^{-3}	100-1000	-	-	-

Adapted from: *http://www.biogas-renewable-energy.info/biogas_composition.html*

Under standard operation, the produced biogas is used to generate: (i) heat at small de-centralised anaerobic plants and; (ii) both heat and electricity through injection into a combined heat and power facility (CHP) at larger plants. This requires selective extraction of both hydrogen sulphide and siloxanes pre-ignition to reduce the impact of internal gas corrosion. However, in response to the instability of the current energy market, both political and economic interest is being shown in understanding the potential of upgrading biogas to natural gas (NG) standards for injection into the national grid and use as a vehicle fuel. This can be achieved by removal of CO_2 from the gas stream and consequently increasing the relative methane content above 90 vol.% (Table 2).

Table 2. Calorific values of methane, biogas and natural gas.

Gas	CH_4 content	Energy density	Energy value	Volumetric equivalence to CH_4
	(vol.%)	(MJ.Nm^{-3})	(kWh.m^{-3})	(-)
Raw biogas	60 - 75	21.5 - 27 [a]	5.97 – 7.5	0.6 - 0.75
Upgraded biogas	+90	32.3 [a]	8.97	+0.9
Natural gas	+95	37.5 - 40 [b]	10.42 – 11.11	+0.95
Methane	100	35.9 [a]	9.97	1

Source: [a] *Constant et al. (1989)*; [b] *National Grid.*

The required purity of upgraded biogas (biomethane) depends on the end use with European standards typically ranging between 95-99 vol.% of methane content. National requirements remain below 6 vol.% and 30 mg.m^{-3} for CO_2 and H_2S, respectively (Table 3).

Table 3. National gas standards for biogas utilisation.

Application	Country	CO$_2$ (vol.%)	O$_2$ (vol.%)	H$_2$ (vol.%)	H$_2$S (mg.Nm^{-3})
Boiler	-	-	-	-	< 1000ppm
CHP	-	-	-	-	< 1000ppm
Gas grid	Germany	< 6	< 3	-	< 30ppm
	Switzerland	< 6	< 0.5	< 5	< 5ppm
Vehicle fuel	Sweden	< 5 [a]	-	-	< 23ppm

Source: *IEA Bioenergy.* [a] Total $CO_2+O_2+N_2$.

Recent studies on anaerobic wastewater treatment under low temperature conditions have indicated that up to 85% of the generated methane can be lost in the liquid effluent due to increased methane solubility (*Barbosa and Sant'Anna, 1989; Kobayashi et al., 1983; Lettinga et al., 1983; Nicholas and Harris, 1997; Noyola et al, 1988; Singh et al., 1996*). For instance, methane concentration at equilibrium with 30 °C water is 16.56 mg.L^{-1}, whilst at 14 °C CH$_4$ content in the liquid phase significantly increases by 70% to 23.56 mg.L^{-1} (Figure 3).
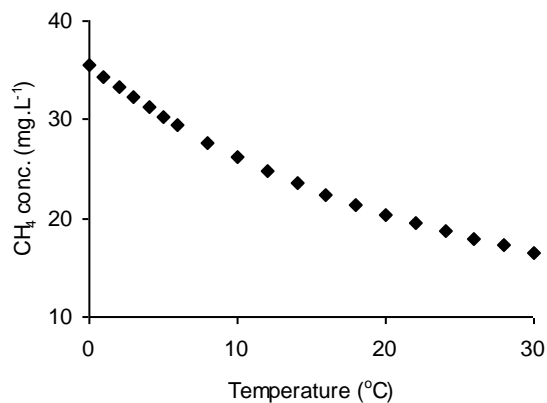
Figure 3. Methane solubility in water as a function of temperature (*Yamamoto et al. 1976*).

New biogas upgrading technologies, such as membrane contactors, have been successfully developed over last two decades, enabling simultaneous removal of CO_2 and H_2S (*Keshavarz et al., 2008*). However, to maximise the amount of generated energy, recovery of dissolved methane from low temperature anaerobic effluent is essential. A few research groups have suggested hollow fibre membrane contactors as a feasible technology (*Bandara et al. 2010*; *Bujalance et al., 2008*).

1.2 Aims and Objectives

The aim of this work was to assess the potential of using membranes to manage methane in wastewater treatment flowsheets with a major emphasis on methane recovery from low temperature anaerobic liquids using hollow fibre membrane contactors (Figure 4).
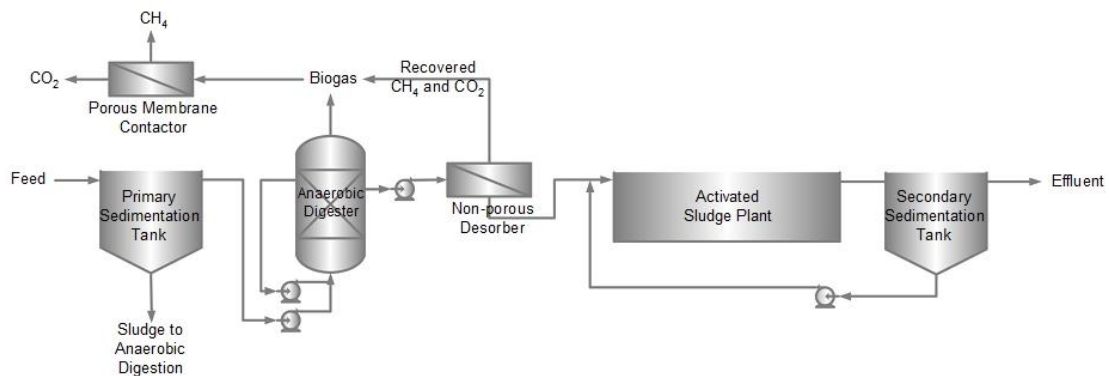
Figure 4. Wastewater treatment flowsheet with incorporated porous membrane contactors for biogas upgrading and dense contactors for dissolved methane recovery.

The specific objectives were to:

(i) Determine the potential for using membrane systems for the de-gassing of methane from wastewater flows.

(ii) Identify optimum operating regimes and process limitations.

(iii) Classify mass transfer characteristics to aid design at full scale.

5

(iv)   Demonstrate the feasibility of the extraction and purification of methane from high rate anaerobic process effluents to use recovered methane as an energy source.

2 Literature Review

2.1 Biogas Upgrading

2.1.1 Upgrading Technologies

Considering the rising price of fossil fuels and pipeline gas, biomethane has been recognised as a potential energy source. To realise European end-product qualities, the purity with respect to upgraded biogas has to reach +96 vol.% of methane content in balance with other trace gases. To achieve this, biogas has to be pre-treated (*i.e.* water vapour and/or sulphur compounds removal) prior to carbon dioxide removal. Current upgrading technologies include pressure swing adsorption (PSA), chemical absorption, physical absorption, membrane permeation and cryogenic separation (Table 4).

Table 4. Comparison of biogas upgrading technologies.

Technology	Status	Pre-treatment	Product purity (vol.%)	CH_4 loss (%)
PSA	Mature	Water vapour, H_2S	> 96	3-10
Water scrubbing	Mature	None	> 97	1-2
Chemical absorption	Mature	Water vapour, H_2S	> 99	0.1
Cryogenic separation	Mature	None	> 99	-
Membrane permeation	Semi-mature	None	-	-

Source*: IEA Bioenergy* and *Smith and Klosek (2001).*

Biogas upgrading technologies have been considered over the past twenty years with plants run successfully worldwide (Table 5). Existing technologies are continually developing due to higher demands put onto product quality, environmental legalisations and cost reduction. Whole life costing incorporating size, energy demand and methane losses indicates that economically viable solutions are only possible at larger scales. New developing

technologies such as membrane contactors (MCs) address these limitations. In particular, the possibility to control the gas and the liquid flow independently enables a constant contact area to be maintained, in contrast to conventional absorption towers, where the mass transfer area varies with liquid loading. Membrane contactors can supply twenty to one hundred times larger surface area per unit volume than packed towers (*Al-Saffar et al., 1997*). Furthermore, membrane contactors reduce practical considerations associated with conventional absorbers such as liquid and gas entrainment, and flooding (*Hoff and Svendsen, 2013*). In addition, MCs were reported to be *ca.* 30 times more efficient in the gas absorption process than their large scale analogues with potential of 65% reduction in the size of the upgrading plant (*Herzog, 2001*). The feasibility studies have demonstrated that the CO_2 can be produced economically from flue gas at small and large scale plants (*CCP; Feron and Jansen, 1999*).

Table 5. List of biogas upgrading plants in selected countries.

Country	Substrate	Biogas utilisation	End-product purity (%)	Upgrading technology	Plant capacity $(Nm^3.h^{-1}_{raw\,gas})$
Austria (Bruck)	Biowaste	Gas grid	97	Membrane permeation	180
Austria (Linz)	Sewage	Gas grid	97	Water scrubber	800
Austria (Pucking)	Manure	Gas grid	97	PSA	10
France (Lille)	Biowaste	Vehicle fuel	97	Water scrubber	2*600
Germany (Utzensdorf)	Biowaste	Gas grid	96	PSA	100
Japan (Kobe)	Sewage sludge	Vehicle fuel	97	Water scrubber	100
Norway (Oslo)	Sewage sludge	Vehicle fuel	-	Chemical scrubber	750
Netherlands (Beverwijk)	Landfill gas	Gas grid	88	Membrane	-
Netherlands (Nuemen)	Landfill gas	Gas grid	88	PSA	1500
Spain (Madrid)	Biowaste	Vehicle fuel	98.5	Water scrubber	4000

Table 5. Cont'd.

Country	Substrate	Biogas utilisation	End-product purity (%)	Upgrading technology	Plant capacity (Nm^3.h^{-1} $_{raw\ gas}$)
Sweden (Boden)	Sewage sludge, biowaste	Vehicle fuel	97	Water scrubber	360
Sweden (Falkengerg)	Sewage sludge, biowaste	Gas grid	97	Chemical scrubber	750
Sweden (Stockholm)	Sewage sludge	Vehicle fuel	97	Chemical scrubber	800
Sweden (Katrineholm)	Sewage sludge	Vehicle fuel	97	Water scrubber	80
Sweden (Malmo)	Sewage sludge	Gas grid	97	PSA	500
Sweden (Uppsala)	Sewage sludge, biowaste	Vehicle fuel	97	Water scrubber	400
Switzerland (Obermeilen)	Sewage sludge	Gas grid	96	Chemical scrubber	100
Switzerland (Samstagen)	Biowaste	Gas grid	96	PSA	50
USA (Renton)	Sewage sludge	Gas grid	96	Water scrubber	4000
United Kingdom (Albury)	Landfill gas	Vehicle gas	-	PSA/Membrane	-

Adapted from *IEA Bioenergy.*

2.1.2 Membrane Contactors for Biogas Upgrading

2.1.2.1 Principle, Applications and Advantages

A membrane contactor device separates liquid and gas flows providing contact at the membrane wall. In porous devices such contact occurs at the pore mouth and negates the need for dispersion, which limits loading rates in the conventional systems. Membrane contactors are typically microporous hollow fibre based membrane systems, in which fluids flow on the opposite sides of the membrane: the fibre (lumen) and the shell side (Figure 5).
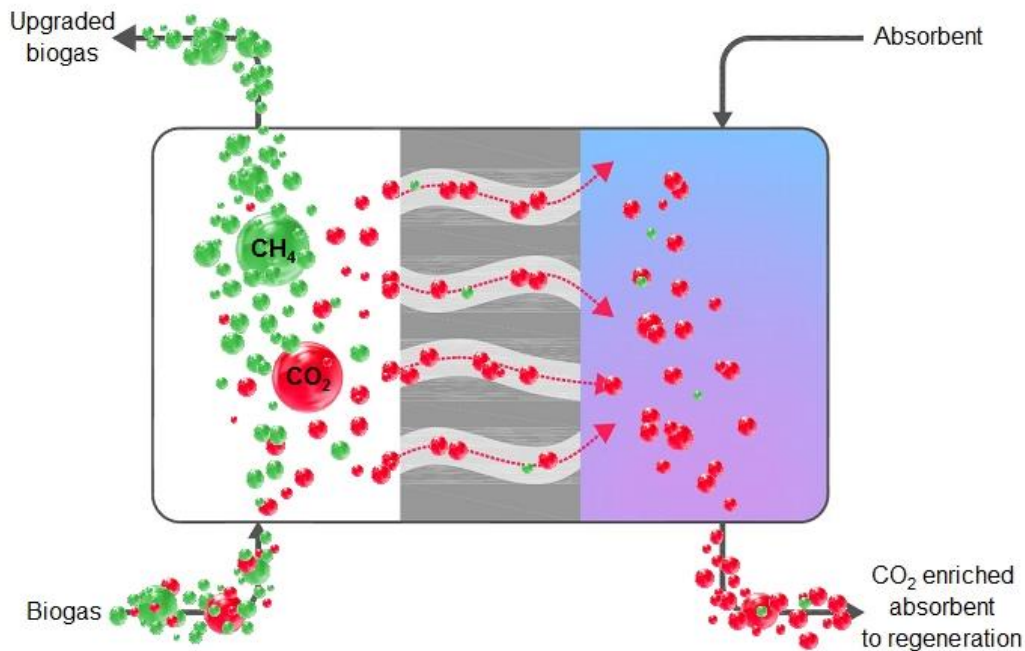
Figure 5. The principle of membrane contactor technology.

To date, membrane contactor technology has principally been applied to high value and low flow rate applications such as blood deoxygenating or industrial scale carbonation of beverages (Table 6).

Table 6. Example applications of porous membrane contactors.

Contacting system	Example applications
Gas / Liquid	Blood deoxygenating; water and beer deoxygenating; ozonation of water; removal of acid gases from digester gas (*i.e.* biogas upgrading); nitrogenation of beer.
Gas / Gas	Dehumidification; volatile organic compounds-air separation.
Liquid / Liquid	Extraction of organic and chlorinated compounds from wastewaters; extraction of fatty acids from oil; extraction of flavours from fruits and vegetables; protein extraction; volatile compounds removal.

Recently there has been some successful development of porous hollow fibre membrane contactors (HFMC) at pilot scale for carbon dioxide extraction from flue gases (*Chen et al., 2001*; *Kumar et al., 2002*; *Lu et al., 2007*; *Rangwala et al., 1996*; *Sea et al., 2002*). Additionally a few studies have reported CO_2 removal from CH_4/CO_2 mixtures (*Husain and Koros, 2007; Ismail and Yaacob, 2006; Simons et al.; 2009*). In this specific application, membrane contactors are an analogous technology to the absorption performed in the packed towers (*i.e.* water and chemical scrubbers). Typically, the absorption liquid comprises an organic amine solution, the purpose of which is to increase the solubility of CO_2 into the liquid and thereby enhance the selection of CO_2 from the gas stream.

The main advantages of membrane contactors over conventional large-scale absorption technologies are: (i) high interfacial contact area provided by the pores and; (ii) a modular design that provides flexibility into application across a wide range of scales. Interfacial areas for membrane contactors were reported by *Matson et al. (1983)* to be up to 10000 $m^2.m^{-3}$, which compares to conventional absorption columns that reach a maximum value of 1000 $m^2.m^{-3}$ (*van Landeghem, 1980)*. Direct comparison between the two revealed CO_2 absorption rates of 1.4 $mol.m^{-3}s^{-1}$ in a membrane contactor with an interfacial area of 1542 $m^2.m^{-3}$ compared to 0.55 $mol.m^{-3}s^{-1}$ in an absorption column with

an interfacial area of 372 $m^2.m^{-3}$ (*Yeon et al., 2005*). These advantages make membrane absorption a promising future technology for biogas upgrading (Table 7).

Table 7. Advantages of membrane contactors for gas absorption.

Advantage	Comments
Modular design	Module compactness results in high contact area, low footprint, low absorbent requirements and a potential of module applicability in small and large plants.
Contact area	Porous material provides high contact area between two phases; surface contact area is constant and known. To compare, in absorption columns random packing results in unknown contact area.
Footprint	Can be applied for de-centralised applications, especially when there is no land available or when absorber requires fitting in confined spaces.
Scaling-up	Due to modular design, membrane contactors scale-up linearly, *i.e.* by employing additional modules in series; as a consequence the scale-up process is simplified.
Absorbent usage	Low absorbent requirements due to small volume of the shell side in comparison with absorption columns; consequently, lower investment and absorbent regeneration cost.
No phase dispersion	By adjusting gas and liquid pressure no dispersion of one phase into another occurs.
No flooding and unloading	No flooding or unloading occurs due to the independency of liquid and gas flow rates, unlike in absorption columns.
No moving parts	Low maintenance and operating cost; safer from health and safety point of view.

The main disadvantages of membrane contactors are:

(i)   The membrane introduces an additional resistance to the diffusing compounds, not found in conventional absorption.

(ii)   Membranes get partially wetted when exposed to the absorbents over a period of time, as a consequence degradation of the membrane surface, which lowers process efficiencies, occurs.

(iii)   Due to partial wetting, the initial performance is unsteady.

(iv)   Module potting is exposed to the attack of the organic solvents leading to a failure in performance.

(v)   Finite lifetime of the membrane requires periodic replacement, resulting in increased investment cost.

The advantages of contactor technology outweigh the process limitations and new, better performing membranes are being developed. Several research groups concentrate on the improvement of the module design and long-term membrane performance (*Atchariyawut et al., 2006; Gugliuzza and Drioli, 2007; Klaassen and Jansen, 2001; Kosaraju et al., 2005; Yang et al, 2005*).

2.1.2.2 Operational Modes

There are two operational modes membrane gas absorption can be performed in: (i) non-wetted mode employing hydrophobic membranes and; (ii) wetted mode employing hydrophilic membranes. In the non-wetted mode membrane pores should remain completely gas-filled; this can be achieved by maintaining slightly higher pressure on the liquid side to prevent gas dispersion into the liquid phase (Figure 6a). In the wetted mode, membrane pores are liquid-filled and gas pressure is kept slightly higher than liquid pressure to prevent formation of liquid droplets in the gas phase (Figure 6b).
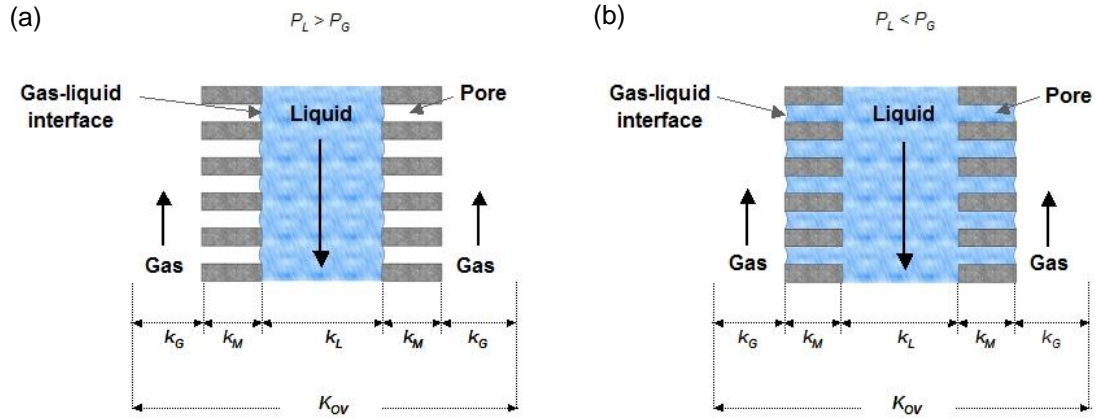
Figure 6. Porous membranes in: (a) non-wetted operational mode; (b) wetted operational mode.

The mass transfer mechanism in both modes consists of three steps: (i) diffusion of gas from the bulk phase into the membrane surface; (ii) gas diffusion through liquid or gas filled membrane pores and; (iii) gas dissolution into the liquid phase boundary layer, where reaction occurs. Several research groups have now demonstrated that the non-wetted mode favours gas mass transfer and consequently results in greater CO_2 fluxes (*Lu et al., 2008; Wang et al., 2005; Yan et al. 2008; Zhang et al., 2008*). In this mode the overall mass transfer resistance (*$1/K_{OV}$*) is described by resistances-in-series model:

$$\frac{1}{K_{OV}} = \frac{1}{k_G} + \frac{1}{k_M} + \frac{1}{Hk_L}$$
(Eq.1)

where K_{OV} is the overall mass transfer coefficient (m.s^{-1}); k_G, k_M, k_L are individual mass transfer coefficients for gas, liquid and membrane respectively (m.s^{-1}); *H* is distribution coefficient of the compound between gas and liquid phase (dimensionless). When a chemical reaction occurs (*e.g.* when amine solutions are employed as absorbents) the liquid phase mass transfer coefficient is expressed as $k_L = Ek_L^0$, where *E* is the enhancement factor for chemical reaction; k_L^0 is physical mass transfer coefficient (s^{-1}).

CO_2 flux (*J_{CO2}*) is concentration-driven and usually expressed as follows (*Boucif et al, 2001*):

$$J_{CO_2} = K_{OV} A \Delta C_{lm} \qquad \text{(Eq.2)}$$

where A is membrane contact area (m^2); J_{CO_2} is gas flux across the membrane (mol.s^{-1}); ΔC_{lm} is logarithmic mean concentration difference (mol.m^{-3}).

In the liquid limited mass transfer the concentration gradient ΔC_{lm} is expressed as (*Das et al., 1998*):

$$\Delta C_{lm} = \frac{(C_{in} - C_{in}^P) - (C_{out} - C_{out}^P)}{\ln \dfrac{(C_{in} - C_{in}^P)}{(C_{out} - C_{out}^P)}} \qquad \text{(Eq.3)}$$

where C_{in} is gas concentration in the feed mixture (mol.m^{-3}); C_{in}^P is gas concentration in the permeate stream at the feed inlet location in equilibrium with gas phase (mol.m^{-3}); C_{out} is gas outlet concentration (mol.m^{-3}); C_{out}^P is gas outlet concentration in the permeate stream at the feed outlet location in equilibrium with gas phase (mol.m^{-3}).

By maintaining gas-filled pores, CO_2 diffusivity through the membrane is increased, *e.g.* the diffusion coefficient of CO_2 in water is 1.92 E-09 m^2.s^{-1} whilst in air it increases to 14 E-06 m^2.s^{-1}. Consequently, additional mass transfer resistance introduced by the membrane can be neglected (*Lu et al., 2008*) and for that reason the majority of the membrane gas absorption processes is performed in the non-wetted modes by utilising polymeric hydrophobic membranes.

2.1.2.3 The Impact of Pore Wetting on Mass Transfer

In practical applications of porous membrane contactors, a decrease in mass transfer is often observed over a prolonged period of time. This phenomenon has been widely reported in the literature and explained by partial wetting of the membrane caused by liquid intrusion into the pores (*Dindore et al. 2004; Franco et al., 2009; Wang et al., 2005*). In general, wetting occurs when the contact angle, θ, between the solid surface and the liquid is less than 90˚, in

which case liquid droplet will spread over a large part of the surface area (Figure 7).

(a)   (b)   (c)
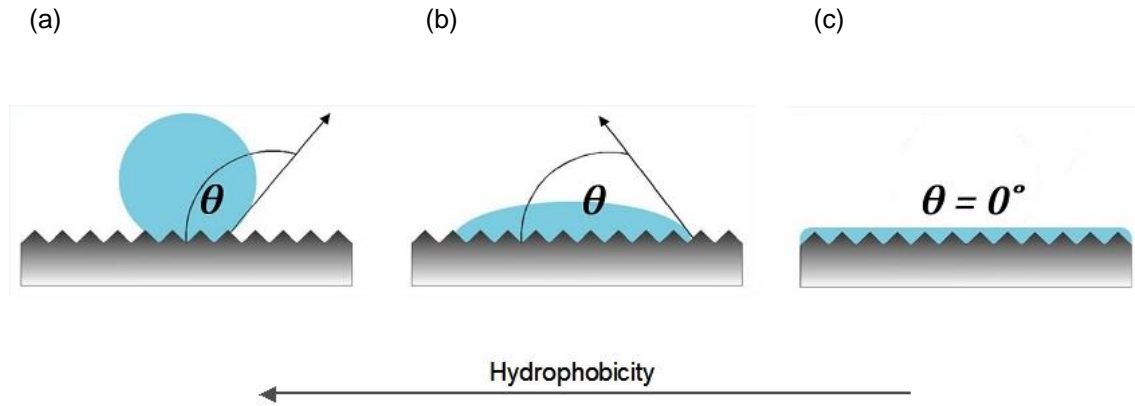
Figure 7. Liquid droplet on porous surface: (a) non-wetted surface, θ > 90 ˚; (b) wetted surface, θ < 90 ˚; (c) completely wetted surface, θ = 0 ˚.

However, in case of microporous structures the intrusion of the liquid into the pores is also dependent on the surface tension and the characteristics of the pores, as stated by Laplace-Young equation:

$$CEP = -\frac{4\gamma \cos \theta}{d_p}$$ (Eq.4)

where *CEP* is the critical entry pressure (kPa); γ is the surface tension (mN.m^{-1}); θ is the contact angle between the solid surface and the liquid (˚); d_p is the pore diameter (m).

The most common and commercially available porous membranes utilised in gas absorption are polypropylene (PP), polytetrafluoroethylene (PTFE) and polyvinyldiene fluoride (PVDF), all characterised by high resistance to wetting (*i.e.* hydrophobicity). To maintain membrane hydrophobicity the critical entry pressure, defined as the pressure at which liquid will enter the membrane pores, should not exceed a certain value. This value depends on the membrane surface energy and liquid surface tension reflected in the contact angle, as previously reported in the literature (Table 8).

Table 8. Critical entry pressure, contact angle and surface tension for PP, PTFE and PVDF membranes and various liquids at 20 °C. Average pore size: 0.2-0.5 μm.

Membrane	Liquid	Surface tension (mN.m^{-1})	Contact angle (°)	CEP (kPa)	Reference
PP	Water	72.30	117.70	90	*Dindore et al. (2004)*
	2 vol.% ethanol	64.18	106.88	-	*Dindore et al. (2004)*
	n-Formyl morpholine	48.14	94.56	> 90	*Dindore et al. (2004)*
	PC	42.00	90.83	78	*Dindore et al. (2004)*
PTFE	Water	72.30	127.42	310	*Dindore et al. (2004)*
	2 vol.% ethanol	64.18	122.10	-	*Dindore et al. (2004)*
	n-Formyl morpholine	48.14	110.80	130	*Dindore et al. (2004)*
	PC	42.00	106.40	110	*Dindore et al. (2004)*
	Water	72.3	-	25.4	*Kumar et al. (2002)*
	MEA	68.2	-	18.2	*Kumar et al. (2002)*
	DEA	64.8	-	14.4	*Kumar et al. (2002)*
	MDEA	57.2	-	13.1	*Kumar et al. (2002)*
	DMEA	49.3	-	12.4	*Kumar et al. (2002)*
PVDF	AMP	-	90.4	-	*Lin et al. (2008)*
	MDEA	-	96.3	-	*Lin et al. (2008*
	PZ	-	76.5	-	*Lin et al. (2008)*

AMP is 2-amino-2-methyl-1-propanol; DEA is dieathanolamine; DMEA is dimethylethanolamine; MDEA is methyldiethanolamine; PC is polycarbonate; PZ is piperazine.

From the above table the following conclusions emerge: (i) membrane hydrophobicity decreases in the following order PTFE < PP < PVDF; (ii) membrane resistance to wetting depends on the type of the liquid that is in the direct contact with membrane surface. Hence, non-wetted operation mode can be maintained by employing compatible absorbents and the adjustment of the trans-membrane pressure (*i.e.* the pressure between gas and liquid phase). However, complexity emerges when taking pore diameter and pore size distribution into consideration. Modelling of membrane gas absorption often assumes regular pore shapes, sizes and pore distribution. In practice, membrane pores are of irregular shape and varying diameters. To demonstrate, up to *c.* 11 times greater maximum pore diameters (d_p) than that of the average have been reported in the literature (Table 9).

Table 9. Average and maximum pore diameter in microporous hydrophobic membranes.

Average pore diameter	Maximum pore diameter	Reference
(μm)	(μm)	
0.31	0.88	*Chittrakarn et al. (2002)*
0.03	0.24	*Lu et al. (2008)*
0.05	0.58	*Lu et al. (2008)*
0.02	0.2	*Yan et al. (2008)*

The significance of this fact is that the predicted value of the critical entry pressure will drop considerably for larger pores; for instance by *c.* 91% for model PP-water system of average d_p 0.05 m and maximum d_p 0.58 m. As a result, a significant fraction of the membrane will initially get wetted due to enhanced liquid penetration into the larger pores. Consequently, the gas-liquid interface (*i.e.* liquid boundary layer when reaction occurs) is shifted to some unknown location inside of the membrane pores, resulting in unknown contact area (*Lu et al., 2008*). Moreover, this leads to liquid stagnation inside the pores

and, subsequently absorbent saturation with carbon dioxide may occur. As a result, dissolved CO_2 cannot be as efficiently extracted from the gas bulk. This phenomenon was confirmed by model analysis of CO_2 concentration distribution in the gas and liquid filled pores (*i.e.* partially wetted membrane) in the work conducted by *Keshavarz et al. (2008)*. They observed that CO_2 concentration builds up in the gas phase near the gas-liquid interface (*i.e.* inside the wetted pores). In addition, the developed model enabled the estimation of flux reduction with time. Membrane wetting significantly reduced CO_2 flux, however the flux reduction was much more intensive at the initial stages of the process; *i.e. c.* 48% of flux reduction occurred when 1% of the pores got wetted. Further wetting, equivalent to the 85% of the liquid intrusion into the pores, resulted in additional 52% flux reduction. However, steady-state (*i.e.* the time at which flux across the membrane stabilises) was reached after 4 days of operation. Similarly, *Mavroudi et al. (2006)* reported a 44% decrease in flux leading to a 55% increase in membrane resistance due to partial membrane wetting. The developed model enabled the estimation of liquid penetration length in relation to the overall pore length as a function of time and therefore the prediction of steady-state. The resistance of the non-wetted part of the membrane (*i.e.* gas-filled pores) was estimated to be 0.3% of the overall mass transfer resistance. The wetted fraction of the membrane contributed to +22% of the overall mass transfer resistance; this effect was further exacerbated at higher liquid velocities (V_L) when resistance of the wetted membrane contributed to 53% of the total resistances. This observation was explained by increased liquid pressure at higher V_L, which led to further liquid intrusion into the pores.

Decreases in the mass transfer coefficient of up to 80% have also been reported in a range of previous investigations (Table 10).

Table 10. Overall mass transfer coefficients and carbon dioxide fluxes for various membranes and absorbents for membrane gas absorption.

		K_{OV}		CO_2 flux			
Membrane	Absorbent	Initial	Steady-state	Initial	Steady-state	Time to reach steady-state	Reference
		E-04 (m.s^{-1})	E-04 (m.s^{-1})	E-04 (mol.m^{-2}s^{-1})	E-04 (mol.m^{-2}s^{-1})	(days, hours or minutes)	
PVDF	Water	-	0.3	10	10	minutes	*Atchariyawut et al. (2006)*
PVDF	2 M NaOH	-	-	32	27	4 days	*Atchariyawut et al. (2006)*
PVDF	2 M MEA	-	-	24	14	11 days	*Atchariyawut et al. (2006)*
PP	PC	0.2	0.07	-	-	-	*Dindore et al. (2004)*
-	DEA	-	-	7.8	5.9	4 days	*Keshavarz et al. (2008)*
PP	1 M MEA	-	-	12.8	6.9	-	*Khaisri et al. (2009)*
PTFE	1 M MEA	-	-	12.9	11	-	*Khaisri et al. (2009)*
PVDF	1 M MEA	-	-	12.9	7.6	-	*Khaisri et al. (2009)*
PP	MDEA	0.6	0.068	-	-	-	*Lu et al. (2008)*
PP	2 M DEA	2.6	0.54	-	-	-	*Lu et al. (2008)*
PP	Water	95	47	25	13.5	13 hours	*Mavroudi et al. (2006)*

Table 10. Cont'd.

Membrane	Absorbent	K_{OV}		CO_2 flux		Time to reach steady-state	Reference
		Initial	Steady-state	Initial	Steady-state		
		E-04 (m.s^{-1})	E-04 (m.s^{-1})	E-04 (mol.m^{-2}s^{-1})	E-04 (mol.m^{-2}s^{-1})	(days, hours or minutes)	
PP	Water	87	47	14	11	4 hours	*Mavroudi et al. (2006)*
PVDF	Water	0.0012	-	0.75	0.75	1 day	*Rongwong et al. (2009)*
PVDF	1 M AMP	0.0039	-	2.95	1.85	-	*Rongwong et al. (2009)*
PVDF	1 M DEA	0.0035	-	3.0	2.0	9 days	*Rongwong et al. (2009)*
PVDF	1 M MEA	0.0084	-	4.0	3.05	9 days	*Rongwong et al. (2009)*
PTFE	MEA	-	-	*c.*10	*c.*3	20 hours	*Seekkuarachchi et al. (2008)*
PP	2 M DEA	2.6	1.55	6.8	5.5	4 days	*Wang et al. (2005)*
PP	2 M DEA	-	-	*c.*5	*c.*4	-	*Zhang et al. (2008)*
PVDF	2 M DEA	-	-	*c.*16	*c.*0.8	-	*Zhang et al. (2008)*

AMP is 2-amino-2-methyl-1-propanol; MDEA is methyl-diethanolamine; MEA is monoethanolamine; NaOH is sodium hydroxide; PC is polycarbonate; PZ is piperazine.

Process stabilisation with time was also reported by *Wang et al. (2005)* in a study involving polypropylene membranes exposed to 2 M diethanolamine (DEA) solution over a time period of 3 months. Overall mass transfer coefficients and CO_2 fluxes were recorded at different days of operation. The initial values of mass transfer coefficient decreased by 15-32% and 23-37% after two and four days, respectively. After this time, the mass transfer coefficient stabilised and constant CO_2 fluxes were observed. At the same time, scanning electron microscopy (SEM) analysis was performed. SEM of the membrane surfaces demonstrated that the DEA solution had partially degraded the PP membrane during the initial four days of exposure beyond which no further morphological changes was observed.

Similar observations were reported by *Dindore et al. (2004)* for polypropylene-polycarbonate system. The exposure of PP membrane to the liquid changed the surface morphology of the membrane. SEM images showed that the number of the smaller pores in polypropylene membrane decreased whilst the larger pores increased in size. This phenomenon was explained by initial wetting of the large pores by the solvent. Absorbent intrusion into the pores exerted lateral force on the pore walls causing the displacement of these walls. The wall displacement resulted in the decreased number of the smaller pores including possible pore blocking.

Irreversible morphological changes of the membrane surface were also observed by *Barbe et al. (2000)* and *Wang et al. (2004)* for polypropylene-water and polypropylene-DEA systems, respectively. Surface degradation greatly increased the possibility of liquid intrusion into the enlarged pores and significantly affected membrane hydrophobicity as reflected in the contact angle. To illustrate, up to *c.* 19% decrease in the contact angle was reported in the literature after membrane exposure to the liquid (Table 11).

Table 11. Contact angle for fresh and degraded polypropylene membranes.

		Contact angle			
		Fresh		Exposed	
Membrane	Absorbent	Water	Absorbent	Absorbent	Reference
		(˚)	(˚)	(˚)	
PP	20 wt.% MEA	128	120	111.2	*Franco et al. (2009)*
PP	20 wt.% MEA + 1000ppm oxalic acid	128	117	103.6	*Franco et al. (2009)*
PP	20 wt.% MEA + 100ppm acetic acid	128	120	104.2	*Franco et al. (2009)*
PP	20 wt.% MEA + 1000ppm formic acid	128	115	109.7	*Franco et al. (2009)*
PP	Water	104.5	N/a	86	*Porcheron et al. (2009)*
PP	20 wt.% DEA	108	103.7	94.5	*Wang et al. (2004)*

MEA is monoethanolamine; DEA is diethanolamine.

Overall, comparison across the reported studies reveals that significant reduction in process efficiencies at the early stages of the operation must be taken into consideration when designing membrane contactors for gas absorption. Even a small amount of liquid intrusion into the membrane pores considerably affects the absorption process, resulting in significantly lower fluxes and mass transfer characteristics.

2.1.2.4 Maintaining Efficient Performance

2.1.2.4.1 Enhancing Reaction Kinetics

In conventional CO_2 absorption mass transfer is enhanced by employing chemical absorbents such as aqueous solutions of AMP (2-amino-2-methyl-1-propanol), NaOH (sodium hydroxide), PC (polycarbonate), PZ (piperazine) and amines: MEA (monoethanolamine), DEA (diethanolamine), MDEA (methyldiethanolamine). The same applies when utilising membrane contactors for carbon dioxide absorption. By introducing chemical reaction higher mass transfers can be achieved in comparison with physical absorption (*i.e.* when employing water as an absorbent). For example, *Lu et al. (2008)* observed an increase in overall mass transfer coefficient from 0.51 E-04 m.s^{-1} to 53.5 E-04 m.s^{-1} when employing 1 M MDEA solution for CO_2 absorption using polypropylene membrane contactor, compared to water. Similarly, *Mavroudi et al. (2003)* obtained *c.* 7 times higher K_{OV} values for 0.5 M DEA in comparison with water.

Higher overall mass transfer rates indicate that the chemical reaction reduces the resistance of the liquid phase boundary layer ($1/k_L$) in comparison with physical absorption. As CO_2 absorption is liquid phase controlled (*Lu et al., 2008; Yeon at al., 2005*), the reduction of liquid phase resistance plays an essential role in enhancing performance. However, when employing chemical absorbents, high decrease of K_{OV} values is often observed over a prolonged period of time. For example, *Lu et al. (2008)* reported up to a 12.5% decrease in K_{OV} when performing CO_2 absorption using PP hollow fibre membrane contactor with MDEA as the absorbent. The same phenomenon was also reported by *Atchariyawut et al. (2007)* for PVDF membrane.

The decrease in mass transfer values when employing chemical absorbents can be explained by wetting tendency of porous surfaces by organic solutions. If liquid comprises organic compounds, even at low concentrations, its surface tension drops rapidly and therefore, as a result of reduced critical entry pressure, partial wetting of membrane is observed (*Dindore et al., 2004*;

Kumar et al., 2002). This results in lower CO_2 fluxes in comparison with the initial values obtained for fresh membranes (Figure 8).
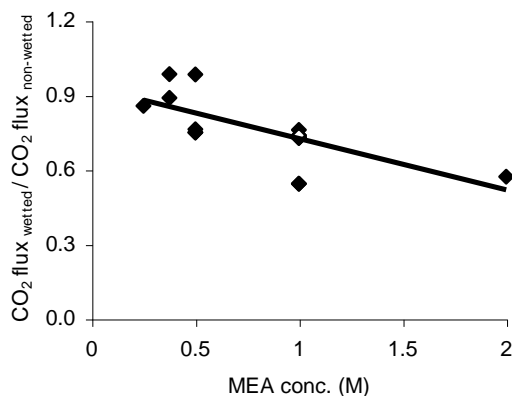
Figure 8. Wetting of porous PVDF and PP membranes as a function of increased MEA concentration. Data collected from: *Atchariyawut et al. (2007)*; *Franco et al. (2009)*; *Rongwong et al. (2009)*. Solid line represents trendline. ♦ PVDF; ◊ PP.

There is a strong relationship between the ratio of membrane wetting and the absorbent concentration. To illustrate, *Lin et al. (2008)* reported *c.* 43% greater liquid intrusion into the PVDF membrane pores when 1 M AMP or 1 M MDEA solution was blended with piperazine. The addition of 0.1 M PZ activator increased liquid viscosity and lowered the value of the contact angle. This enhanced wetting of the membrane pores resulted in a decrease in K_{ov} by 36% and 39% for AMP and MDEA, respectively. Conversely, PZ addition resulted in up to 93% greater values of CO_2-amine reaction enhancement factor, *E*. Due to the enhanced reaction in the liquid phase boundary layer (inside of partially-wetted membrane pores) up to 34% lower fractional liquid phase resistances were reported.

Other studies also emphasised the fact that enhancement of the chemical reaction, either by increasing molar concentration of absorbents or by the addition of activators, greatly increases process efficiencies (Table 12).

Table 12. The effect of increased absorbent concentration on membrane performance.

Membrane	Absorbent	Absorbent concentration		Increase in selected parameter	Reference
		Lowest (M)	Increased (M)		
PP	NaOH	0.0005	0.01	6% increase in CO_2 removal efficiency	*Al-Marzouqi et al. (2008)*
PVDF	NaOH	0.1	1.0	9% increase in CO_2 flux	*Atchariyawut et al. (2007)*
PVDF	NaOH	1.0	2.0	3% increase in CO_2 flux	*Atchariyawut et al. (2008)*
PTFE	MEA	1.0	3.0	42% increase in CO_2 flux	*Khaisri et al. (2009)*
PVDF	1M AMP + PZ	0.1	0.4	24% increase in k_M	*Lin et al. (2008)*
PP	DEA	0.5	1.0	20% increase in K_{OV}	*Mavroudi et al. (2003)*
PP	DEA	0.5	2.0	28% increase in K_{OV}	*Mavroudi et al. (2003)*
PP	DEA	0.5	2.0	51% increase in CO_2 recovery	*Rangwala (1996)*
PVDF	MEA	0.25	0.5	36% increase in CO_2 flux	*Rongwong et al. (2009)*
PVDF	MEA	0.25	1.0	50% increase in CO_2 flux	*Rongwong et al. (2009)*

It is often observed that blended amine solutions appear to be the most-compatible absorbents when taking process efficiencies into consideration. For instance, *Yeon et al. (2005)* demonstrated that by employing a MEA/TEA hybrid solution, 90-95% process efficiencies could be achieved over a period of 3 days. In contrast, *c.* 23% lower efficiencies were achieved when pure MEA absorbent was employed. *Lu et al. (2007)* reported up to 22% greater CO_2 fluxes for hybrid MDEA/PZ and MDEA/AMP absorbents in comparison with values obtained for pure MDEA. The greater performance of blended amine absorbents can be explained by the increased reaction rate constants (k_R). To illustrate, k_R for PZ is as high as 15336 (*Sun et al., 2005*), AMP k_R is 955 (*Xu et al., 2007*), whilst MDEA k_R is only 3.91 (*Ko and Li., 2000*).

Whilst highly concentrated absorbents enhance most reaction kinetics, the unsteady performance at the initial stages of operation can be a limiting factor that prevents membrane contactors from large-scale, long-term industrial applications. One pragmatic solution is to significantly increase gas side pressure when the process reaches steady-state. To illustrate, *Wang et al. (2005)* increased gas pressure from 0 to 8.3 kPa, consequently CO_2 flux was maintained at 90% of the initial flux value. On the other hand, over-pressure on the gas side may result in the bubble formation (*Dindore et al., 2004*).

Another suggestion is to design larger contactor units aimed to treat gas streams under steady-state conditions. This solution, however, increases investment and operational costs due to increased amount of membrane material and absorbent required. Therefore, the studies undertaken by researchers focus on: (i) the identification of compatible absorbents; and (ii) the development of novel membranes.

2.1.2.4.2 Long-term Absorbent Performance

In order to maintain long-term steady performance, absorbent loading capacities and possible interactions between the membrane and absorbent solution must be taken into consideration. In general, CO_2 loading capacities of the commercially available amine absorbents increase in the following order:

MEA > DEA > MDEA (*Barzagli et al., 2010; Rongwong et al., 2009*). The tendency of porous membranes being wetted by these solvents decreases in the same order, as reflected in liquid surface tension (refer to Table 8, section *2.1.2.3*). On the other hand, amine solutions of high CO_2 loading capacity are more corrosive (*Wang et al., 2004*). Consequently, membrane potting and the membrane itself are exposed to the attack of chemical absorbent.

Work conducted by *Franco et al. (2009)* outlined the fact that amine degradation is one of the main problems in amine-based membrane gas absorption. Due to amine reaction with CO_2, absorbents undergo irreversible degradation (*Kohl and Nielsen, 1997; Strazisar et al., 2003*). The products of amine degradation (polymerised carbamates) have high molecular weight and subsequently affect liquid viscosity, which may lead to high pressure drop inside the module (*Franco et al., 2009*). Moreover, the exposure of membrane to the degraded solvent reduces membrane hydrophobicity. To illustrate, *Franco et al. (2009)* reported a *c.* 13% lower contact angles for PP membrane exposed to a degraded MEA solution (containing oxalic, acetic and formic acids) in comparison with fresh MEA.

Another problem associated with long-term absorption performance is the loss of volatile amines from the aqueous solutions, due to gradual permeation of volatile compounds through the porous membrane. The occurrence of this phenomenon led to a search for alternative non-volatile absorbents. For example, *Kosaraju et al. (2005)* employed a novel absorbent polyamidoamine (PAMAM) dendrimer for CO_2 scrubbing using PP hollow fibre membrane. The employment of highly hydrophobic liquid resulted in consistent mass transfers over a period of 55 days. In contrast, mass transfer coefficient obtained for MEA solution decreased by *c.* 40% over a period of 65 days; however the addition of fresh MEA to the absorbent solution retrieved the value of initial K_{OV}.

2.1.2.4.3 Wetting Prevention

Attempts to eliminate wetting has led to research on ideal interfaces in membrane gas-liquid contacting systems. Efforts have been put into fabrication of asymmetric membranes that can maintain long-term steady performance. New methods of membrane preparation, such as non-solvent induced phase inversion separation (NIPS) or coating porous membranes with ultra-thin dense layer, have been proposed. For instance, in the work conducted by *Atchariyawut et al. (2006)* PVDF membranes were produced by adding pore forming additives to the casting solution. Depending on the additive, the membranes contained an outer or inner dense skin layer. It was found that the membrane of long "finger-like" shaped pores with ultra-thin outer dense skin layer is the most resistant to wetting. Consequently, this membrane was characterised by highest overall mass transfer coefficient (3.5 E-05 $m.s^{-1}$) and CO_2 flux (*c.* 1.35 E-03 $mol.m^{-2}s^{-1}$). To compare, K_{OV} of commercially available PVDF membrane, with irregular pore shapes and double dense skin layers, was reduced by *c.* 40%; CO_2 flux was reduced by *c.* 30%.

In the work conducted by *Gugliuzza and Drioli (2007)* HYFLON AD solution was used to produce highly hydrophobic PVDF membranes with contact angles as high as 141°. One of the biggest membrane manufacturers, Milipore, provides plasma treated PVDF membranes with super-hydrophobic properties, *i.e.* membrane surface is characterised by the contact angle higher than 150°. These modifications result in reliable long-term performance of gas-liquid contacting systems (Table 13).

Table 13. The performance of treated porous membranes in gas-liquid contacting process.

Membrane	Manufacturer	Absorbent	Contact angle (˚)	Selected Parameter Reduction	Run time	Time to reach steady-state	Reference
PP	Membrana GmbH modified	Water	123	Max. 1% reduction in contact angle value	2 min	-	*Yang et al. (2005)*
PP	Membrana GmbH modified	Water	149	No reduction	2 min	-	*Yang et al. (2005)*
PTFE	Milipore, plasma treated	1 M AMP	135*	3% reduction of the initial recovery	30 days	5 days	*Lin et al. (2009)*
PVDF	Home made by NIPS	Water	-	Up to 1% reduction in initial flux	15 days	-	*Atchariyawut et al. (2006)*
PVDF	Milipore	1 M AMP	133*	1% reduction of initial recovery value	10 days	10 days	*Lin et al. (2009)*
PVDF	Milipore, plasma treated	1 M AMP	155*	No reduction	30 days	-	*Lin et al. (2009)*

*Contact angle for water

A few studies emphasised the fact that additional dense skin layer increase membrane mass transfer resistance and hence overall mass transfer resistance (*Li and Teo, 1998; Poddar et al., 1996*). However, providing that the thickness of membrane coating is less than 10 E-06 m, it doesn't significantly influence the overall mass transfer coefficient (*Kreulen et al., 1993*). For instance, less than 5% increase in membrane mass transfer resistance was reported by *Xu et al. (2004)* when PTFE membranes were coated with thin layer of sodium alginate hydrogel.

The performance of the porous membranes, however, is also determined by the symmetry of the porous support and the pore size distribution. The former relates to the presence of inner dense skin layers, inside of porous polymer matrix, which when present increases membrane mass transfer resistance (*Gugliuzza and Drioli, 2007*). As for the latter, the presence of large pores increases the possibility of liquid intrusion into the pores. New techniques enabling the formation of membranes with regular shaped and sized pores are being developed; *e.g.* bombarding of polymers with neutrons (*Chittrakarn et al., 2002*).

2.2 Methane Recovery from Liquids

2.2.1 Principles of Membrane De-gassing

De-gassing of liquids is a mature technology proven at industrial scale in a wide range of applications such as water deoxygenating or removal of nitrogen from water used in fish hatcheries. In conventional de-gassing towers, trays or random packing provides a contact area between liquid containing dissolved gases with a vacuum employed to drive gas release. Porous membrane contactors have been used for the same purpose; however, membrane technology outweighs the limitations of conventional de-gassing. The advantages of membrane de-gassing devices (desorbers) over a conventional vacuum towers are analogous to advantages of membrane contactors utilised as gas absorbers (see section *2.1.2.1*); however, the fundamentals of the process differ. In membrane de-gassing, vacuum or sweep

gas flows on one side of the membrane wall enabling extraction of dissolved gases from the liquid bulk; purified liquid flows on the other side of the membrane and is constantly removed in order to enhance concentration-driven mass transfer.

Porous membrane contactors have been successfully applied for de-gassing applications at industrial scale, *e.g.* blood and water deoxygenating. Recent pilot-scale studies showed the potential of membrane degassers when employed as carbon dioxide desorbers in hybrid absorption-desorption installations (*Bhide et al, 1998*; *Simons et al., 2009*). This suggests that membrane desorbers could be a potential engineering solution for the recovery of dissolved methane from anaerobic effluent. However, due to the nature of anaerobic liquids, the surface of porous membrane could be strongly affected by the presence of solid particles (*i.e.* membrane fouling) and wetting phenomenon. Hence, for this specific application non-porous membranes seem to be an optimal solution.

2.2.2 Selection of Compatible Membranes

The principle of the de-gassing process using porous and non-porous membranes remains the same; the difference lies in the transport of gaseous compounds through the membrane. The mass transport across non-porous membranes is described by the solution-diffusion model consisting of three steps: (i) the dissolution of gas into the non-porous membrane; (ii) the diffusion of gaseous compound through the membrane; and finally (iii) re-dissolution of gas penetrant into the gaseous phase (Figure 9).
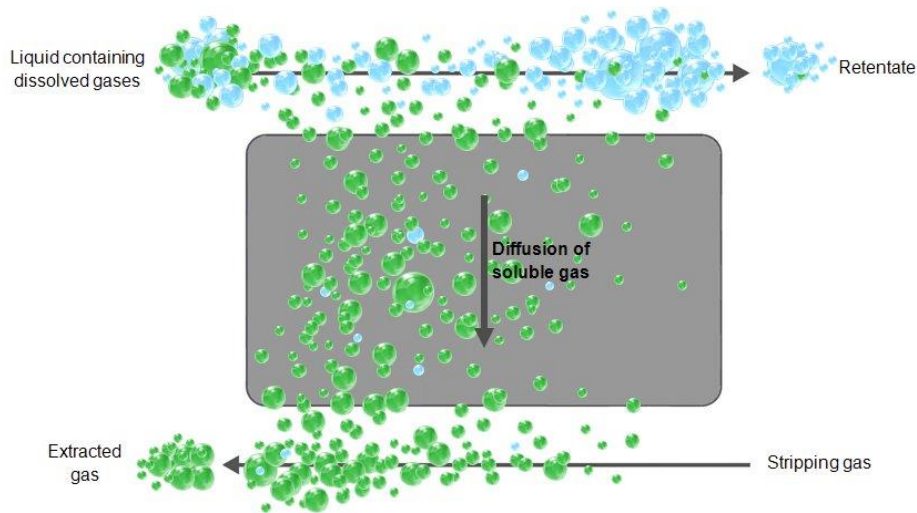
Figure 9. Mass transport through non-porous membrane.

The permeability of gas molecules, *P*, through the membrane is a function of: (i) the solubility of gas in the membrane material, *S*, and; (ii) gas diffusivity through the membrane, *D*; and can be expressed by the following approach:

$$P = SD \tag{Eq.5}$$

The former, *S*, depends on penetrant affinity to the membrane material. The latter, *D*, depends on the physical properties of the membrane and the penetrating molecule. In general, rubbery polymers are much more permeable to gases than glassy polymers (Table 14).

Table 14. Permeability of gases through rubbery and glassy polymeric membranes.

Polymer	Gas permeability				Reference
	CO_2	CH_4	O_2	N_2	
	(Barrer)				
Silicone rubber [a]	3200	940	600	280	*Bodzek (2000)*
Silicone rubber [a]	3800	1200	800	400	*Merkel et al. (2000)*
Silicone rubber [a]	4550	1430	781	351	*Stern (1994)*
Silicone rubber [a]	1330	85	-	-	*Tremblay et al. (2006)*
Silicone rubber [a]	3230	950	620	280	*Robb (1986)*
Natural rubber [a]	130	28	-	-	*Bodzek (2000)*
Natural rubber [a]	-	-	24	-	*Robb (1986)*
Polypropylene [b]	-	-	1.6	0.3	*Bodzek (2000)*
High-density polyethylene [b]	-	-	1.0	-	*Robb (1986)*
Cellulose acetate [b]	6.0	0.19	-	-	*Bodzek (2000)*
Cellulose acetate [b]	4.75	0.15	0.82	0.15	*Stern (1994)*
Polysulfone [b]	4.4	0.16	-	-	*Bodzek (2000)*
Polyimide [b]	0.2	0.003	-	-	*Bodzek (2000)*
Polyamide [b]	0.16	0.014	-	-	*Bodzek (2000)*

[a] - rubbery polymer; [b] - glassy polymer. 1 Barrer = $10E^{-10}$ cm^3STPcm.$cm^{-2}s^{-1}cmHg^{-1}$.

The difference in permeability between the two groups of polymers can be explained by rigidity of the polymers as reflected in glass-transition temperature, T_g, (Table 15).

Table 15. The glass-transition temperature of rubbery and glassy polymers.

Polymer	Symbol	T_g (˚C)	Reference
Poly-di-methyl-siloxane [a]	PDMS	-123	*Charati and Stern (1998)*
Poly-propyl-methyl-siloxane [a]	PPMS	-120	*Charati and Stern (1998)*
Poly-tri-fluoro-propyl-methyl-siloxane [a]	PTFPMS	-70	*Charati and Stern (1998)*
Poly-phenyl-methyl-siloxane [a]	PPhMS	-28	*Charati and Stern (1998)*
High-density polyethylelene [b]	PE-HD	-23	*Bodzek (2000)*
Polypropylene [b]	PP	-10	*Bodzek (2000)*
Polyisopropene [b]	IR	205.15	*Tremblay et al. (2006)*
Matrimix polyimide [b]	PI	313	*Bos et al. (1998)*

[a] - rubbery polymer; [b] - glassy polymer.

With a decrease in T_g, rotational (intrasegmental) mobility of the polymeric chains increases, enhancing gas diffusion through the polymeric membrane (*Charati and Stern, 1998*). This phenomenon can be explained by the structure of polymers, *i.e.* the size of surrounding chains attached to the main polymer chain. For instance, poly-di-methyl-siloxane (PDMS) has two methyl groups attached to the silicone atom. In contrast, in poly-propyl-methyl-siloxane (PPMS) one of the methyl groups is replaced by bulkier propyl group (Figure 10). As a result, the mobility of the bulkier side chain is reduced and consequently lower gas diffusivities are observed.
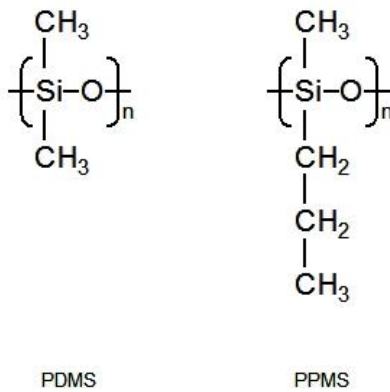
Figure 10. Structure of selected polymeric membranes.

Out of all commercially available rubbery polymers, poly-di-methyl-siloxane is characterised by the highest chain mobility. This suggests that PDMS membranes are the most-suitable materials in terms of achieving highest gas permeabilities.

2.2.3 Diffusion of Methane through PDMS Membranes

The diffusion mechanism through silicone membranes is usually described by "free-volume" theory (*Stern, 1994*). The "free-volume" (microactivity) is an empty space of the polymer matrix surrounded by the side chains (Figure 11). The movements of the side chains enable penetration of the gas molecules into the polymer. The oscillating gas molecule resides inside of the microactivity for a period of time, until the cooperative motions of the surrounding side chains open a "pathway" to the next microactivity; in which case the molecule "jumps" into the neighbourhood microactivity, providing it is not occupied by other gas molecules.
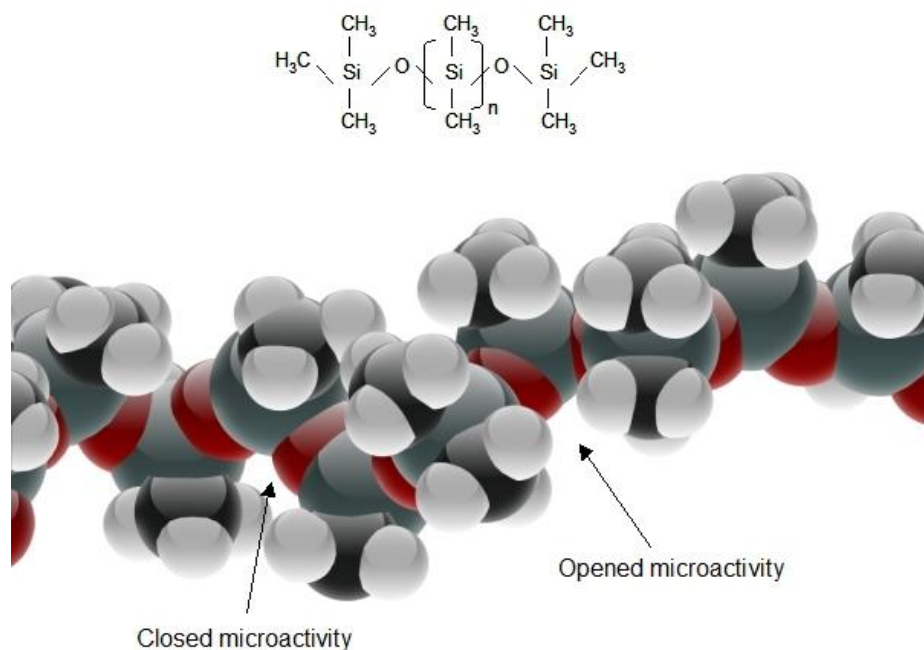
Figure 11. Poly-di-methyl-siloxane chain.

The dynamics of the microactivities depend on the length of the side chains, however, the amount and the distribution of fractional "free-volume" also plays an essential role in the process of gas diffusion. Work conducted by *Charati and Stern (1998)* enabled the estimation of "free-volume in silicone polymers. It was found that the amount of fractional "free-volume" increases with chain mobility, and that the distribution of microactivities changes more frequently with the decrease in length of side chains, as follows: PDMS ≥ PPMS > PTFPMS > PPhMS. In addition, the diffusion coefficient of methane increased in the same order, underlining the potential applicability of PDMS membranes for dissolved methane recovery (Table 16). Moreover, the diffusivity of carbon dioxide through PDMS, another principal compound present in the anaerobic effluent, is relatively high, suggesting that simultaneous recovery of both gases could be conducted.

Table 16. Diffusion coefficients of methane and carbon dioxide through silicone membranes.

Gas	Diffusion coefficient E-06 (cm^2.s^{-1})				Reference
	PDMS	PPMS	PTFPMS	PPhMS	
CH$_4$	24	8.1	5.6	1.2	*Charati and Stern (1998)*
CH$_4$	18	-	-	-	*Raharjo et al. (2007)*
CH$_4$	12.7	-	-	-	*Robb (1986)*
CH$_4$	20.6	-	-	-	*Tamai (1994)*
CO$_2$	26	11	5.3	2.0	*Charati and Stern (1998)*
CO$_2$	11.0	-	-	-	*Robb (1986)*

The variations in the values of diffusivity coefficient through PDMS are due to different process conditions.

2.2.4 Mass Transfer in Non-porous Membranes

The overall resistance to mass transfer is described by resistances-in-series model, and for non-porous membranes is expressed by the following approach (*Aptel and Semmens, 1996*):

$$\frac{1}{K_{OV}} = \frac{1}{k_L} + \frac{1}{k_M m} + \frac{1}{k_G H} \qquad \text{(Eq.6)}$$

where K_{OV} is overall mass transfer coefficient; (m.s^{-1}); k_L, k_M, k_G are individual mass transfer coefficients for liquid, membrane and gas phase, respectively (m.s^{-1}); m is the partitioning coefficient of the compound between membrane and the liquid phase; H is a distribution coefficient of the compound between gas and liquid phase (dimensionless).

Mass transfer resistance in non-porous membranes depends on membrane-permeant compatibility (*i.e.* the solubility of the compound in the membrane material) and the diffusivity of the compound through the membrane.

For non-porous hollow fibre membranes, the membrane mass transfer resistance is also dependent on the geometry of the module, and can be expressed as follows (*Cocchini et al., 2002*):

$$R_M = \frac{1}{k_M} = \frac{r_i \ln(r_o / r_i)}{D_M m_M}$$ (Eq.7)

where R_M is membrane mass transfer resistance (s.m^{-1}); r_i is the inner radius of the hollow fibre; r_o is the outer radius of the hollow fibre (m); D_M is the diffusivity coefficient of the permeant through the membrane (m^2.s^{-1}); m_M is partitioning coefficient of the compound between the membrane and liquid solution (dimensionless).

Experimental measurement of membrane resistance can be determined by plotting overall mass transfer resistance (*1/Kov*) against $V_L^{-\alpha}$ (*Wilson, 1915*):

$$\frac{1}{K_{ov}} = cV_L^{-\alpha} + \frac{1}{k_M m}$$ (Eq. 8)

where *c* represents a constant; *α* is an empirical constant that provides the best straight line; intercept represents membrane resistance.

The mass flux across the membrane is expressed by the following approach (*Cussler, 1984*):

$$J = K_{OV} (C-C^*)$$ (Eq.9)

where *J* is the mass flux (mg.m^{-2}.s^{-1}); *C* is the concentration of the compound in the bulk liquid (mg.L^{-1}); *C** is the equilibrium concentration of the compound in the gas phase (mg.L^{-1}).

2.2.4.1 Mass Transfer Correlations

Mass transfer correlations enable the prediction of membrane performance under various hydrodynamic conditions and aid engineering

design of the membrane modules in order to achieve highest process efficiencies. In general, and for membrane systems in particular, mass transfer correlations are expressed by the following approach:

$$Sh = a\ Re^{b}\ Sc^{c}$$ (Eq.10)

where *a*, *b*, *c* are the values dependent on the operating conditions and the geometry of the membrane module.

Sherwood number (*Sh*) is a function of mass diffusivity ($K_{OV}.d_h$) and molecular diffusivity (*D*), and is expressed by the following equation:

$$Sh = \frac{K_{OV}d_h}{D}$$ (Eq.11)

where d_h is the hydraulic diameter of the shell or the lumen side, dependent on the module characteristics and operational mode.

Reynold's number enables the comparison of dynamic similarity of different membrane systems, and is expressed as follows:

$$Re = \frac{Vd_h\rho}{\mu}$$ (Eq.12)

where *V* is the fluid velocity (m.s^{-1}); ρ is the density of the fluid (kg.m^{-3}); μ is the viscosity of the fluid (Pa.s).

Schmidt number is a function of kinetic viscosity of the fluid and molecular diffusivity, represented by the following equation:

$$Sc = \frac{\mu}{\rho D}$$ (Eq.13)

A number of mass transfer correlations, strongly dependent on the operation regime (*i.e.* lumen or shell feed mode), hydrodynamics of the system, geometry of the module and properties of the employed fluids have been developed (Table 17). However, whilst these correlations can predict the mass

transfer, the models are inappropriate for the prediction of membrane performance under unsteady conditions (*e.g.* different temperatures and inlet concentrations).

Table 17. Mass transfer correlations for transfer of volatile compounds through polymeric membranes.

Process	Membrane	Mode	Correlation	Model validity	Reference
Organic/aqueous extraction	Non-porous	Lumen feed	$Sh = 0.0225\ Re^{0.8} Sc^{0.33}$	$500 < Re < 5000$	*Doig et al. (1999)*
Organic/aqueous extraction	Non-porous	Shell feed	$Sh = 0.0408\ Re^{0.8} Sc^{0.33}$	$500 < Re < 5000$	*Doig et al. (1999)*
Water deoxygenating	Non-porous	Lumen feed	$Sh = 1.615\ ((d_h/L)ReSc)^{0.33*}$	$Re < 2000$	*Tan et al. (2005)*
Water deoxygenating	Non-porous	Shell feed	$Sh = 3.228\ Re^{0.5632} Sc^{0.33}$	$Re < 10$	*Tan et al. (2005)*
Water deoxygenating	Porous	Shell feed	$Sh = 0.53\phi\ Re^{0.53} Sc^{0.33}$	$21 < Re < 324$	*Costello et al. (1993)*
CO_2 absorption	Porous	Shell feed	$Sh = 0.39\ Re^{0.59} Sc^{0.33}$	$1.4 < Re < 5.3$	*Ferreira et al. (1998)*
Water deoxygenating	Porous	Shell feed	$Sh = 1.25\ Re^{0.93}\ (d_h/L)^{0.93} Sc^{0.33}$	$Re\ (d_e/L) < 1000$	*Yang and Cussler (1986)*
Pervaporation of chloroform/water solutions	Porous with dense skin layer	Shell feed	$Sh = 0.89\ Re^{0.48} Sc^{0.33}$	$1 < Re < 100$	*Crowdwer and Cussler (1998)*

ϕ is hollow fibre module packing density; * Levaque solution (*Levaque, 1928*).

3 Methodology

3.1 Headspace Gas Chromatography Analysis

3.1.1 Headspace Gas Chromatography

In the present study, concentration measurements were conducted by headspace gas chromatography (HS-GC) was applied. The method enables the identification and quantitation of light volatiles and semi-volatiles (*e.g.* methane, carbon dioxide) dissolved in the liquid. Chemical compounds partitioned from liquid into the headspace are injected into a previously calibrated gas chromatograph. The concentration of the solutes is determined from the chromatogram peak.

3.1.2 Materials

Methane and carbon dioxide at 5, 24.97, 49.97 and 74.99 vol.% in balance with nitrogen (Scientific Technical Gases Ltd, UK) were utilised as standards. Helium of 99.996 vol.% purity (BOC, UK) was used as the GC carrier gas.

3.1.3 Standard Preparation

Methane and carbon dioxide liquid standards were prepared by filling a 22.7 mL (±0.02 mL) glass vial with de-ionised water such that no bubbles were present. The samples were sealed with chlorobutyl/PTFE caps (Chromacol, UK) and left overnight to reach laboratory temperature (19.5 $\pm$0.5 °C). The headspace was created by replacing 5 mL of water with 5 mL of calibration gas of known concentration, using simultaneously two 10 mL glass tight syringes (SGE, Australia). The samples were shaken on a centrifuge at 2060 rpm for 7 minutes and left overnight for 13-16 hours enabling gas equilibration. Extracted gas was manually injected into the gas chromatograph using 1 mL gas tight syringe (SGE, Australia). Both the gas and liquid standards were analysed 5

times. CH_4 and CO_2 recovery was determined from previous calibration of the chromatograph.

3.1.4 Method Development and Validation

The bubble extraction method was adapted from *Walsh and McLaughlan (1999)* with optimisation of the bubble equilibrium time and agitation technique. Five sample replicates (*n* = 5) were prepared with a model gas containing 24.97 vol.% methane in balance with nitrogen.

To estimate equilibrium time, samples were generated according to the procedure described in section *3.1.3* and analysed within the range of time from 0 to 25 hours. Methane saturation occurred and remained stable after 13.5 hours (Figure 12). Under the experimental conditions, *i.e.* T=19 °C, p=1.013 Bar, dissolved methane concentrations were 20.88 mg.L^{-1} (±0.22). To compare, *Yamamoto et al. (1976)* obtained the value of 20.8 mg.L^{-1}. To ensure equilibrium has been reached, standards and real samples have been left for 14+ hours.
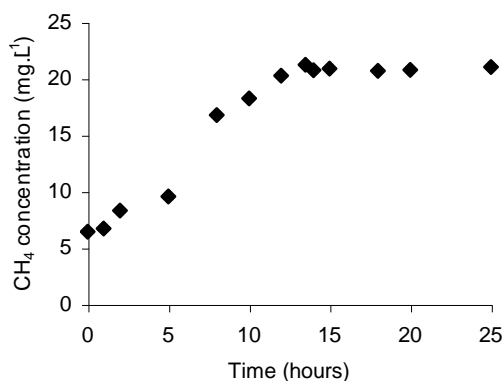
Figure 12. Methane concentration as a function of bubble equilibrium time.

The degree of agitation required to maximise recovery from the liquid phase standards was evaluated by variations in shaking time and shaking speed. Once shaking time exceeded 3.5 minutes, recovery remained stable (Figure 13a). To ensure consistency in recovery, a time of 7 minutes (double that of the initial identified point of optimum recovery) was adopted.
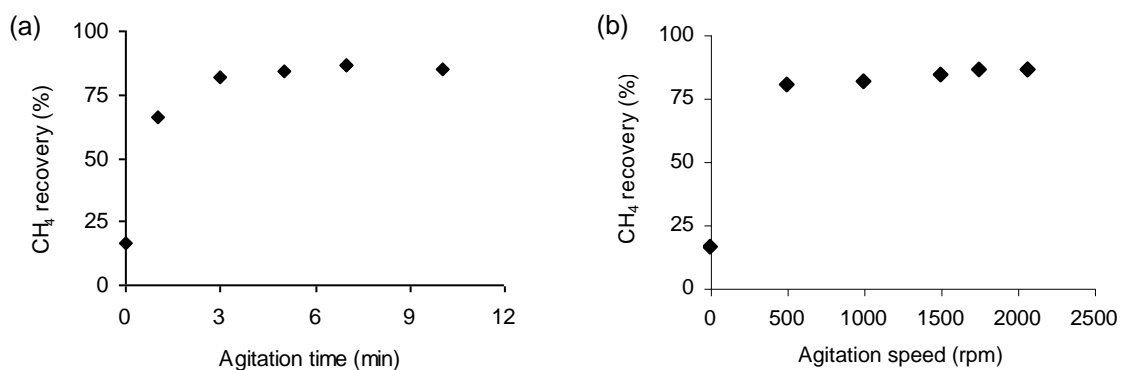
Figure 13. Methane concentration as a function of: (a) agitation time; (b) agitation speed.

The effect of agitation speed was established by increasing centrifuge shaking speed. Once shaking speed exceeded 500 rpm, recovery remained stable enabling 80 $\pm$5% methane recovery (Figure 13b). Maximum speed of 2060 rpm, resulting in the lowest standard deviation of 1.7%, was chosen to ensure consistency in recovery.

The method was validated by evaluating linearity, accuracy and repeatability of the results according to the procedure described by *Kim et al. (2006)*. The extraction efficiency was estimated within the range of 5 - 74.99 CH_4 vol.% (Table 18).

Table 18. The linearity and accuracy of the developed method ($n = 5$).

Solute	Solute concentration (vol.%)	Correlation coefficient	Intercept	Average recovery (%)	Average SD (%)	Detection limits (vol.%)
CH_4	5.0 – 74.99	0.9997	0.1144	80	0.79	1.2

The intercept of 0.9997 validated the precision of the method. The standard deviations (SD) were greater at higher gas concentrations; for

46

instance SD at 5% injected gas volume was 0.96% whilst for 75% injected volume exceeded the value of 2.2%.

3.1.5 Calibrations

Gas and liquid CH_4 and CO_2 calibration curves were obtained with an average of peak area ratios from replicates. The linearity was determined in the range 0.99 - 74.99 vol.% and 5 - 74.99 vol.% for CH_4 and CO_2, respectively (Figure 14a and b).
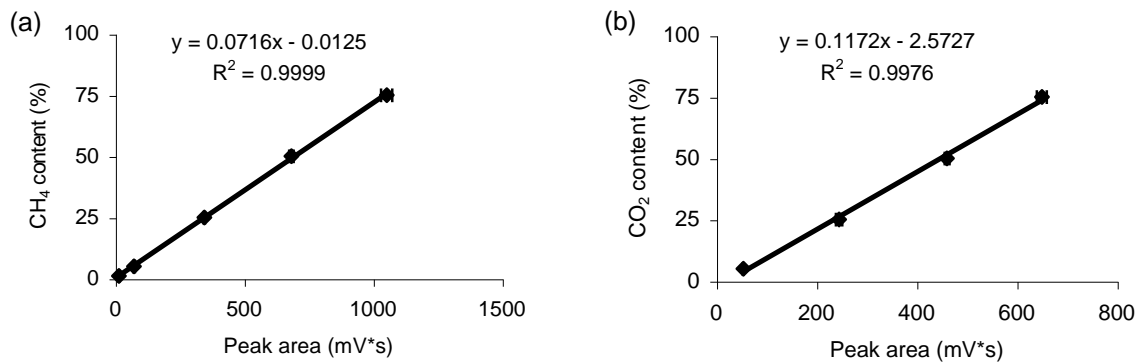
Figure 14. Calibration curves determined from standard gases for: (a) methane (b) carbon dioxide.

For standard gases, correlation coefficients (R^2) were higher than 0.997; relative standard deviations varied between 0.5-2%.
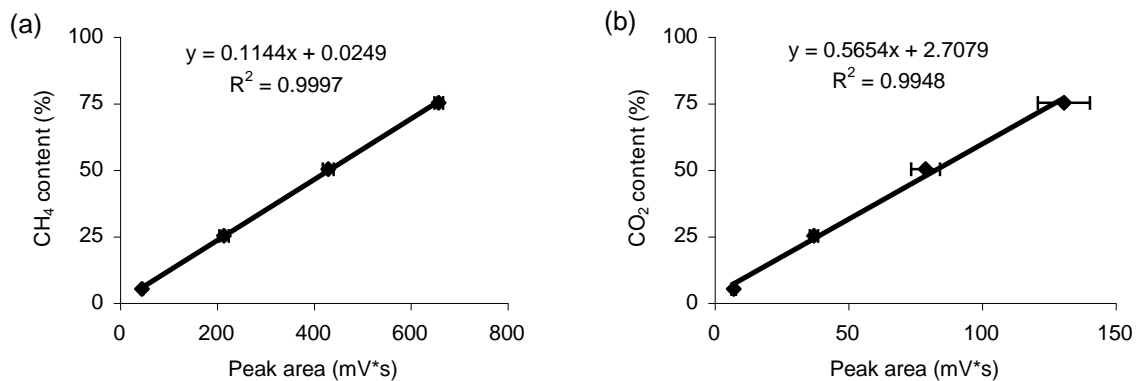
Figure 15. Calibration curves determined from 5 mL of standard injected into the water: (a) methane liquid phase; (b) carbon dioxide liquid phase.

Standard solutions of dissolved methane and carbon dioxide were prepared according to the procedure described in section *3.1.3.* Obtained calibration curves (Figure 15a and b) were used to quantify concentrations of gases in real samples. The curves were linear with correlation coefficients higher than 0.99 and relative standard deviations up to 2.6% for methane and 7.5% for carbon dioxide.

3.1.6 Instrumentation

Sample analysis was conducted on 200i Series GC (Cambridge Scientific Instruments, UK) fitted with a thermal conductivity detector (Figure 16a) and CTR I Concentric Packed Column (Alltech, UK). A CTR is a column within a column enabling separation of the volatile chemical compounds (Figure 16b). The outer column (6ft x 1/4"), packed with activated molecular sieve, allowed separation of oxygen, nitrogen and methane; inner column (6ft x 1/8"), packed with porous polymer mixture allowed separation of methane and carbon dioxide.
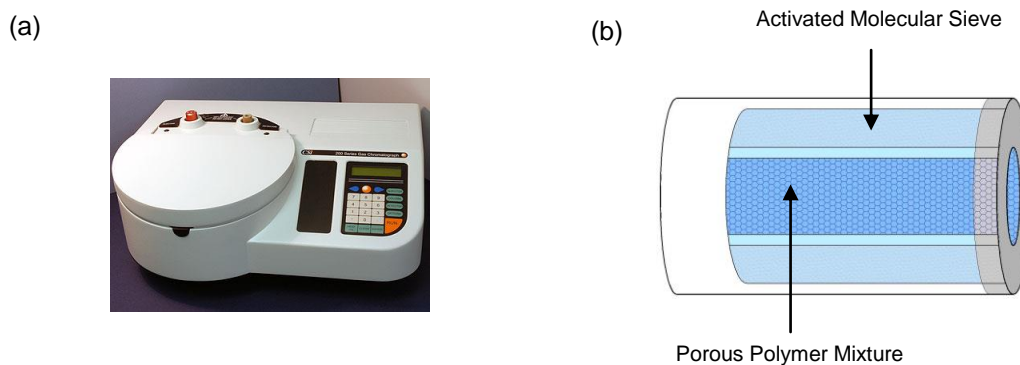
Figure 16. Head-space gas chromatography: (a) gas chromatograph; (b) CTR I concentric column enabling separation of the mixture of the extracted solutes.

The retention times for carbon dioxide, oxygen, nitrogen and methane were 0.82, 1.7, 2.18 and 3.52 minutes, respectively. Helium gas at 5.0 psi was used as a carrier gas; oven temperature was held isothermal at 100 °C; detector and injector temperature were set up at 120 °C.

3.1.7 Quantitation of Dissolved Gases by Gas Chromatography

Dissolved gases concentration was calculated using a mass balance approach (*Hartley and Lant, 2006*):

$$X_{L1} = \frac{X_{G2}(Vol_G + \alpha Vol_L) - X_{G1}Vol_G}{Vol_L}$$

(Eq.14)

where X_{L1} the concentration of dissolved gas in solution (mg.mL^{-1}); X_{G1} is the concentration of gas in headspace before shaking (mg.mL^{-1}); X_{G2} is the concentration of gas in headspace after shaking and at equilibrium (mg.mL^{-1}); Vol_G is the volume of headspace (mL); Vol_L is the volume of liquid in the vial (mL); α is Bunsen solubility coefficient for each specific gas, depended on the temperature.

The volume of the vial was determined by mass difference before and after filling the vial with the sample:

$$Vol_V = \frac{(M_F - M_E)}{\rho_L}$$

(Eq.15)

where Vol_V is the volume of vial (mL); M_F is the mass of liquid filled vial, and cap (mg); M_E is mass of an empty vial and cap (mg); ρ_L is the solution density at experimental temperature (mg.mL^{-1}).

Volume of headspace gas was determined as follows:

$$Vol_G = Vol_V - Vol_L$$

(Eq.16)

$$Vol_L = \frac{M_L - M_E}{\rho_L}$$

(Eq.17)

where M_L is the mass of the capped vial filled with liquid, with headspace created above the liquid solution (mg).

3.2 PDMS De-gassing Module

3.2.1 Module Fabrication

Poly-di-methyl-siloxane (PDMS) pre-oxide tubes (Sterilin, UK) were utilised as hollow fibre membranes and housed inside of the poly-vinyl-chloride (PVC) clear tube (International Plastic Systems Ltd, UK). As the module performance relies on the bonding forces between potting material and: (i) PDMS hollow fibres; (ii) PVC shell; it was crucial to identify temperature and pressure resistant adhesives. Prior to module construction several resins have been tested to ensure strong bonding characteristics as any leak could lead to the intrusion of one phase into another, resulting in false experimental data.

PDMS fibres were fixed inside a PVC module shell using rubber sealant (Dow Corning S.A., Belgium) and epoxy resin (Crystal Resin, Gedeo, UK) mixed with polyolefin primer (Loctite 770, Henkel, Germany). A 3 mm thick layer of Blu Tack (Bostik, UK) was utilised to separate silicone rubber from the resin at the potting end. Araldite (Huntsman Advanced Materials, USA) was used to seal the T-piece and socket connectors (Pipeline Centre Plastics, UK) to PVC module shell (Figure 17). Prior to use the developed module was tested for gas and liquid leaks.
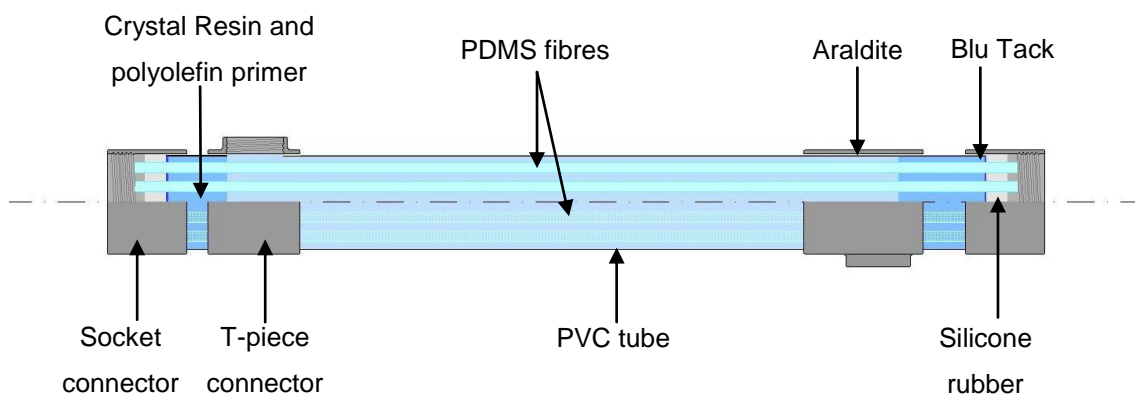
Figure 17. Poly-di-methyl-siloxane membrane module.

3.2.2 Module Characteristics and Post-treatment

Once the optimal potting method was chosen, membrane modules were built for specific synthetic and anaerobic application. Three different membrane modules were tested in order to identify the impact of membrane wall thickness and module packing density on methane recovery (Table 19).

Table 19. PDMS module characteristics used for extraction of methane from synthetic and anaerobic liquors.

Experiments	Module	Wall thickness (mm)	Outside diameter (mm)	Inside diameter (mm)	Number of fibres (-)	Module length (m)	Contact area (m^2)
Synthetic	1	0.25	3.7	3.2	13	0.62	0.094
Synthetic	2	1.0	5.2	3.2	7	0.81	0.093
Anaerobic	3	1.0	5.2	3.2	10	0.85	0.139

To avoid membrane clogging de-ionised water at 720-780 mL.min^{-1} flow rate was pumped through the module for 3 minutes before and after each set of experiments.

3.3 Synthetic Experiments

3.3.1 Water Saturation

To produce a synthetic anaerobic solution the method from *Walsh and McLaughlan (1999)* was adapted. De-ionised water (ELGA, UK) in equilibrium with air was used, and 99.995% pure CH_4 and 99.8% pure CO_2 (BOC, UK), passed through the liquid at various CH_4/CO_2 compositions to saturate prior to use (Figure 18). The aspirator tank (Fisher Scientific, UK) was filled with 22 L of de-ionised water, leaving 2 L of headspace above and rubber stopper was used to seal the system (Figure 19a). Methane and carbon dioxide gases were

introduced through tube 1 and 2, respectively. Tube 3 connected the saturator with a glass jar enabling gas withdrawn to avoid over-saturation of the liquid as pressure increased in the system. During all experimentation tube 3 was kept below the water level in the glass jar to ensure no air entered the system.
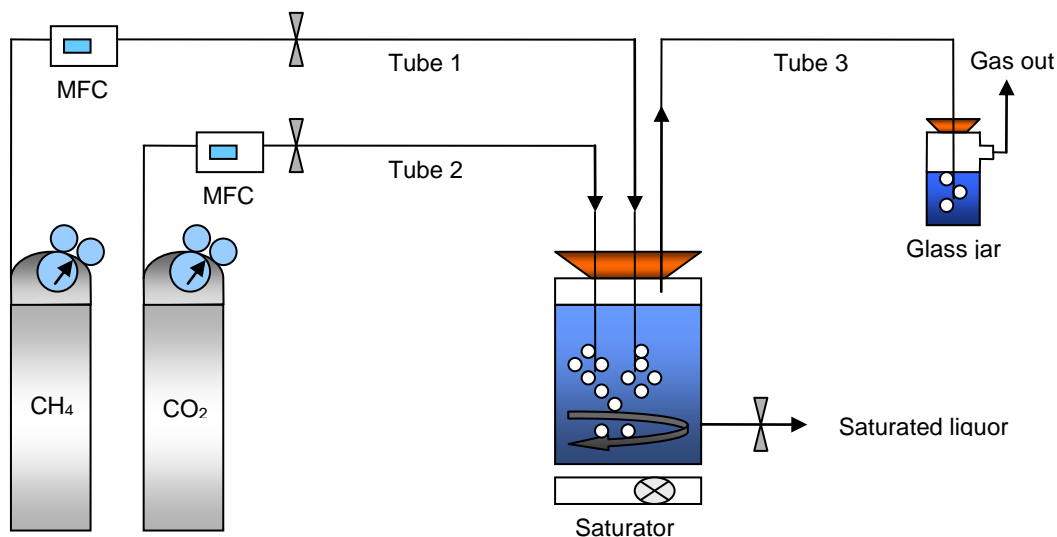
Figure 18. Water saturation experimental set-up.

To enhance mass transfer of gaseous solute into the water, a magnetic stirrer (Model SB161, Stuart, UK) was placed at the bottom of the saturator. Positive gas flow was kept through all the experimentation to ensure gases equilibration in liquid.

Figure 19. Equipment used for water saturation with methane and/or carbon dioxide: (a) water saturator; (b) sparging head.

Pure gases or a binary mixture of CH_4/CO_2 was introduced into the liquid at total flow of 0.6 L.min^{-1}. Water saturation at 19 °C occurred after *c.* two hours when present in isolation, resulting in concentrations of 21 mg.L^{-1} for CH_4 (Figure 20a) and 1642 mg.L^{-1} for CO_2 (Figure 20b). The obtained results are in agreement with data reported by *Yamamoto et al. (1976)* and *Weiss (1974)* for CH_4 and CO_2, respectively.
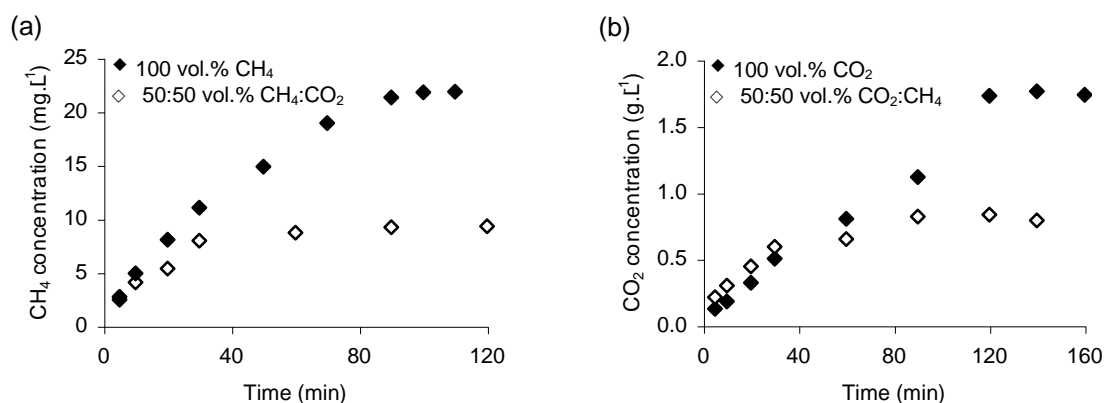
Figure 20. Methane and carbon dioxide saturation in water: (a) 100 vol.% methane and 50:50 vol.% methane in balance with carbon dioxide; (b) 100 vol.% carbon dioxide and 50:50 vol.% carbon dioxide in balance with methane.

3.3.2 Experimental Rig Set-up

3.3.2.1 Sweep Gas De-gassing

Water containing various concentrations of the solutes, was introduced into the shell side of the PDMS membrane module via a peristaltic pump (624s, Watson Marlow, UK) at flow rates varying from 4 mL.min^{-1} to 780 mL.min^{-1}. Nitrogen gas with a purity > 99%, generated from compressed air using a dense gas separation membrane (*McAdam and Judd, 2008*), was applied as a stripping medium enabling extraction of dissolved gases (Figure 21). The gas flow rate was controlled in the range of 0.2 L.min^{-1} to 21 L.min^{-1} using a needle valve flow gauge (RS Components, UK); the gas pressure was measured with pressure transducers (Sensit, Roxspur Measurement and Control Ltd, UK).
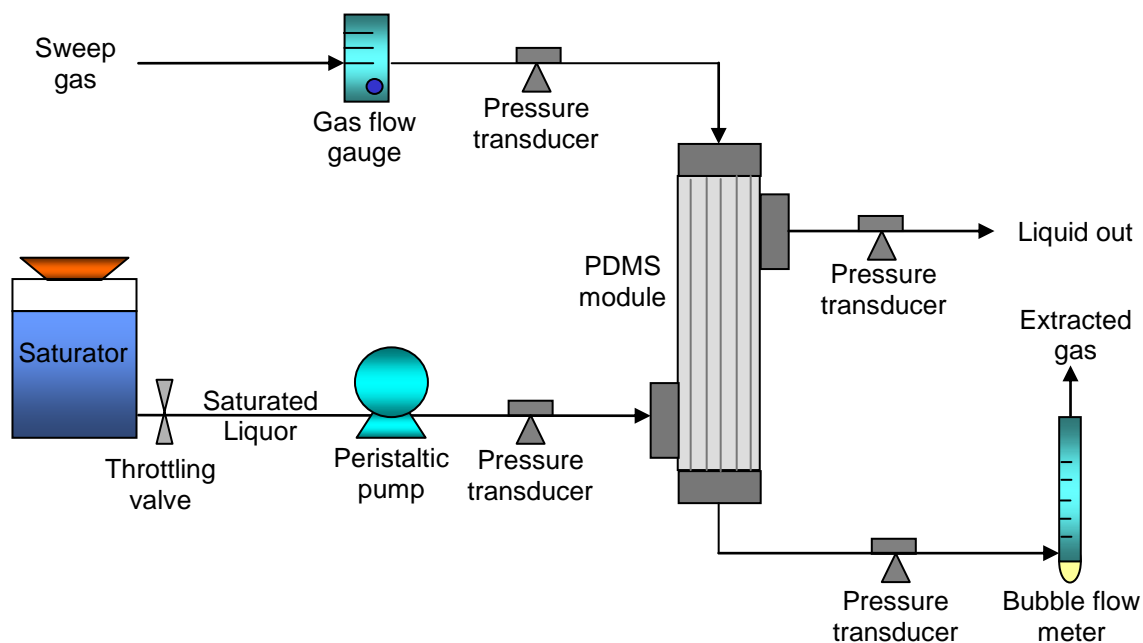
Figure 21. Experimental set-up for synthetic sweep gas de-gassing; gas was introduced into the lumen side while liquid was introduced counter-currently into the shell side.

The outlet gas flow was measured using a 50 mL soap film bubble flow meter (Restek, UK). Liquid and gas samples were collected in pre-evacuated sealed vials after three retention times. Based on the hydraulic conditions tested, steady-state was reached between 1-120 minutes, dependent upon liquid velocity. Collected samples were analysed by gas chromatography via manual injection of 1 mL volume of the sample headspace into the chromatograph sampling port.

3.3.2.2 Vacuum De-gassing

Vacuum conditions were generated by connecting a vacuum pump (Model no: 420-1902, Thermo Scientific, UK) onto one side of the membrane module and creating a dead end on the other side (Figure 22). A needle valve (Swagelok, UK) enabled regulation of the vacuum pressure within a range 0 to 308 mBars. Water containing dissolved gases was introduced into the shell side counter-currently to the vacuum. Liquid flows varied from 6 mL.min^{-1} to 780 mL.min^{-1}.
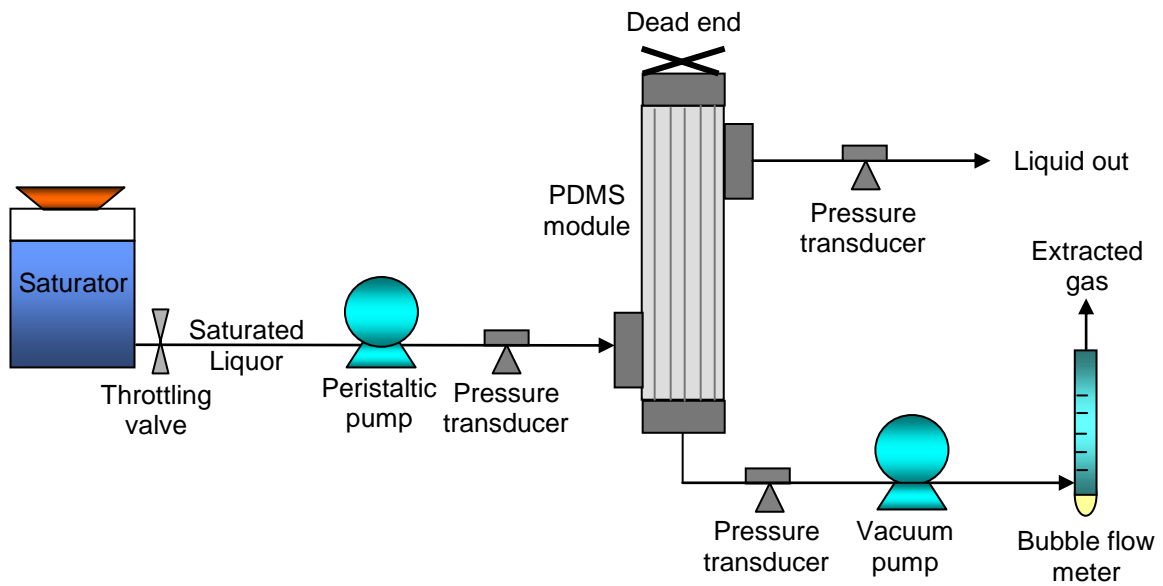
Figure 22. Experimental set-up for synthetic vacuum de-gassing; gas was introduced into the lumen side while liquid was introduced counter-currently into the shell side.

One of two variables, *i.e.* liquid flow rate or vacuum pressure, was kept constant, enabling identification of the optimum mass transfer characteristics under vacuum operational mode. Samples were collected according to the procedure described in the section *3.3.2.1*.

3.4 Anaerobic Experiments

3.4.1 Expanded Granular Sludge Blanket (EGSB) Reactor

Effluent was taken from a parallel experiment on anaerobic sewage treatment conducted at Cranfield University's sewage treatment works. Over the period of operation, the wastewater feed comprised an average of 360 mgtCOD.L^{-1}, 161 mgsCOD.L^{-1}, 210 mgBOD.L^{-1} and 123 mgTSS.L^{-1} (n = 15). The EGSB reactor (Figure 23) comprised a cylindrical vessel with a 42.5 L working volume, 1.5 m hydraulic depth and 0.19 m diameter (Paques, The Netherlands). A three-phase separator was integrated for retention of particulates and comprised a two-stage lamella clarifier and subsequent overflow weir. The hydraulic retention time (HRT) was maintained at 9.4 hours resulting in a total chemical oxygen demand (tCOD) loading of 0.9 kgCOD m^{-}

^{3}.d^{-1}. In addition, the EGSB design incorporated an external recirculation pump (620s, Watson Marlow, UK) to maintain upflow velocity independent of HRT at 1.2 m.h^{-1}. The EGSB reactor was seeded with 25 L of granular sludge from a paper mill.

Figure 23. Expanded Granular Sludge Blanket reactor.

The EGSB was operated for 248 days in total. The data reported within this study represents a cumulative experimental period of 57 days. During the experimental period, temperature averaged 16 °C (±1 °C). Gas flow rate was consistently recorded using a micro wet-test gas volume meter (TG01, Ritter, Bochum, Germany) and gas composition monitored using a portable infra-red analyser (LMS Xi G2, Gas Data Limited, Coventry, UK).

3.4.2 General Analytical Parameters

Total and soluble COD were analysed using Merck Spectroquant cell tests with subsequent detection by spectrophotometry. Reactor temperature was monitored using an on-line sensor (Endress and Hauser, Germany) and manual temperature readings of the effluent recorded daily.

3.4.3 Experimental Rig Set-up

Anaerobic effluent comprising dissolved methane and carbon dioxide was pumped into the shell side of the membrane module (*Module 3*; Table 19, section *3.2.2*) using a peristaltic pump (624s, Watson Marlow, UK). Liquid flow rate was controlled in the range of 40 mL.min^{-1} to 780 mL.min^{-1} (liquid velocity, V_L, 0.0033 m.s^{-1} to 0.064 m.s^{-1}). Nitrogen sweep gas was introduced counter-currently into the membrane lumen. Gas flow rate was controlled in the range of 0.6 L.min^{-1} to 15 L.min^{-1} (gas velocity, V_G, 0.125 m.s^{-1} to 3.11 m.s^{-1}) using a needle valve flow gauge (RS Components, UK). Three retention times passed prior to sampling to ensure steady-state had been reached. Based on the hydraulic conditions tested, steady-state was reached between 0.3 minutes and 5.7 minutes, dependent upon V_L.

Under vacuum operational conditions, liquid flow rates were kept in the range 0.6 L.min^{-1} to 15 L.min^{-1}. Vacuum pressure was generated using vacuum pump (Model no: 420-1902, Thermo Scientific) and varied from 0.0 kPa to 30.8 kPa. Prior to sampling steady-state conditions has been reached.

For the experimental set-up, please refer to the section *3.3.2*.

3.4.4 Developing the Sampling Technique

Prior to real sample collection, two sampling methods were considered: (*Method 1*) slow vial filling with the liquid so no bubbles occur, followed by sample sealing and laboratory based headspace generation (*Walsh and McLaughlan, 1999*); (*Method 2*) capping the glass vial and evacuating the sealed system prior to sample collection (*Alberto et al., 2000*). The accuracy of the sampling technique (Table 20) was determined through the on-site sample collection, followed by analytical analysis described in section *3.1.3*.

Table 20. Precision of the sampling method in real sample for lowest and highest liquid flow rate.

Q_L (mL.min^{-1})	Method 1		Method 2	
	CH$_4$ conc. (mg.L^{-1})	SD (*n=10*) (mg.L^{-1})	CH$_4$ conc. (mg.L^{-1})	SD (*n=10*) (mg.L^{-1})
6	12.2	0.3	12.3	0.2
780	6.7	1.4	12.3	0.3

The estimated methane content at low liquid flow rates (6 – 80 mL.min^{-1}) was equivalent for either *Method 1* or *Method 2*. For higher liquid flow rates (100 – 780 ml.min^{-1}), the value obtained via *Method 1* dropped by *c.* 55% compared to *Method 2*. In addition, when sampling by *Method 1*, standard deviations were magnified by *c.* 21% at high liquid flow rates. This can be explained by equilibrium disruption while filling the vial with liquid at high flows.

As the *Method 2* enabled more precise sampling, it was chosen as an on-site sampling technique. Capped vials were pre-evacuated using a vacuum pump (Capex L2C, Charles Austin Pumps, UK) allowing vacuum generation up to 280 mBar. Vacuum conditions enabling 5 mL headspace creation were established at maximum pump flow rate Q_L 8.0 L.min^{-1}, and occurred after 15 seconds (Figure 24a and b).
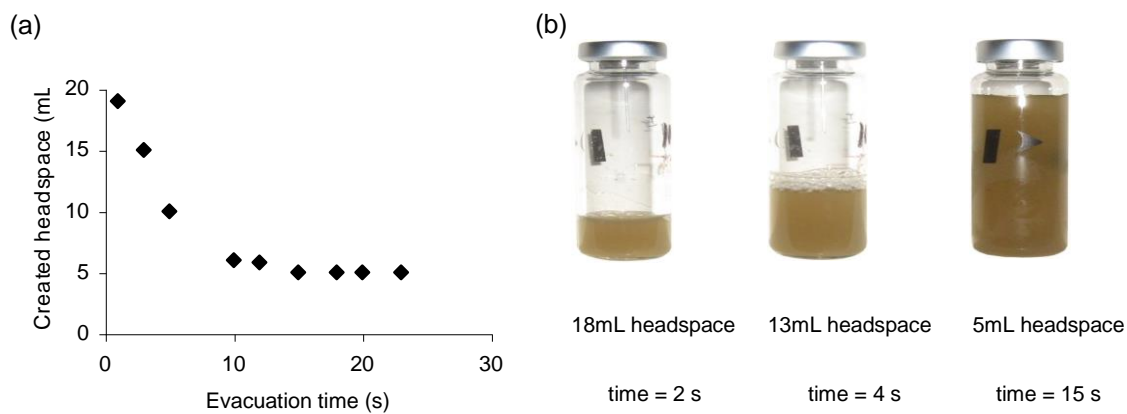
Figure 24. Gas headspace obtained by Method 2: (a) headspace as a function of evacuation time; (b) liquid and gas phase in sealed vials as a result of evacuation time.

The samples were collected in triplicate via in-situ needle injection through the septum; the created suction pressure enabled liquid intake into the vial and further chromatography analysis. Prior to real sample analysis, gas and liquid standards were injected into GC in triplicate.

4 Results and Discussion

4.1 Methane Recovery from Synthetic Liquids

4.1.1 The Effect of Liquid Hydrodynamic Conditions on Pure Methane Recovery

In order to estimate mass transfer characteristics, a series of experiments were performed. Firstly, the significance of liquid hydrodynamic conditions on pure methane recovery was investigated. Water saturated with methane passed through the shell side of the membrane module at velocities varying from 0.00017 to 0.0472 m.s^{-1} (*Re* 1.3 - 344); sweeping gas or vacuum was applied counter-currently as a stripping medium. In sweep gas operation the highest process efficiency of 93% was recorded under the lowest V_L tested at 0.00036 m.s^{-1} (Figure 25a), equivalent to 2.1 (SD ±0.6) mg.L^{-1} CH$_4$ as an outlet concentration (Figure 25b). Analogous results were obtained under vacuum conditions, *i.e.* the highest extraction efficiency of *c.* 78 % was recorded under lowest V_L of 0.0017 m.s^{-1}, equivalent to 4.0 (SD ±1.3) mg.L^{-1} CH$_4$ as an outlet concentration. In both operational modes, process efficiency decreased by *c.* 88% and *c.* 46% (sweep gas and vacuum mode, respectively) at the highest liquid velocity tested. This indicates that recovery efficiency is proportional to the liquid retention time in the module shell side. At low liquid velocities the developed liquid phase boundary layer facilitates gas build up near the membrane surface; this develops a concentration gradient across the PDMS membrane and consequently enhances methane diffusivity through the membrane. At higher V_L, methane dissolution into the membrane decreases due to reduced liquid retention time, subsequently resulting in lower gas diffusivity. *Ito et al. (1998)* and *Tan et al. (2005)* similarly observed higher removal efficiencies at lower liquid velocities when using PDMS hollow fibre membrane contactors for de-oxygenation of water.

In terms of methane molar fluxes, no significant differences between sweep gas and vacuum de-gassing were recorded under liquid velocities below

0.0061 m.s^{-1} (*Re* 44). For intermediate V_L of 0.024 m.s^{-1} (*Re* 175) the recorded CH$_4$ molar fluxes in sweep gas operation increased by *c.* 80% to the value of 0.031 mol.m^{-2}.s^{-1}; vacuum operation resulted in *c.* 95% greater CH$_4$ molar flux, equivalent to 0.037 mol.m^{-2}.s^{-1}. When employing the highest V_L of 0.0472 m.s^{-1}, the vacuum operation resulted in 81% higher CH$_4$ molar fluxes, in contrast with values of 0.09 mol.m^{-2}.s^{-1} obtained in sweep gas operation (Figure 25c).
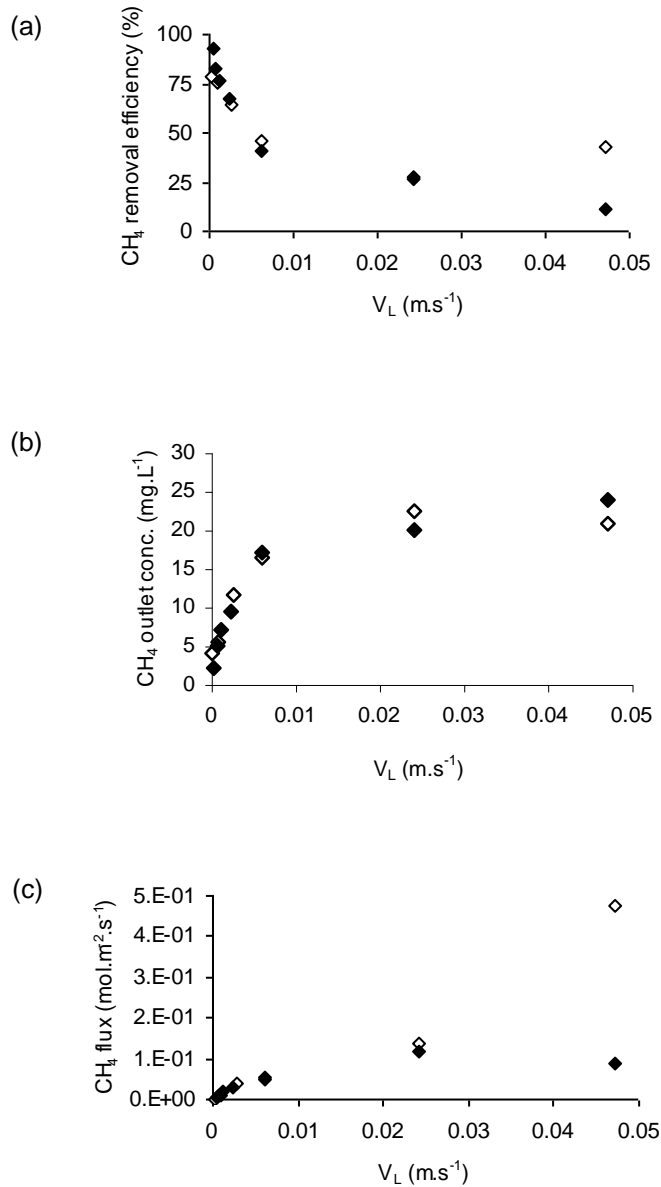
Figure 25. Pure methane recovery from water as function of liquid velocity: (a) methane removal efficiency; (b) methane outlet concentrations; (c) methane molar flux. ◆ Sweep gas, V_G = 0.033 m.s^{-1}; ◇ Vacuum, P_{vac} = 24 mBar.

Significant differences in CH_4 fluxes and recoveries obtained under highest V_L for the two operational modes can be explained by the sensitivity of the process to the concentration of dissolved gas in the liquid feed. To demonstrate, when employing water containing 36.2 (SD ±3.9) $mg.L^{-1}$ of dissolved methane, the obtained methane fluxes reached 0.48 $mol.m^{-2}.s^{-1}$ (vacuum mode at highest V_L). The inlet methane concentration in sweep gas operation at the highest V_L was 26.7 (SD ±0.8) $mg.L^{-1}$; hence the obtained CH_4 fluxes considerably dropped to the value of 0.09 $mol.m^{-2}.s^{-1}$. However, it is worth noting that employing highest V_L in sweep gas operation resulted in *c.* 13% greater CH_4 outlet concentration in comparison with the vacuum mode. This unexpected change in the trend is a result of data normalisation, *i.e.* methane outlet concentration is not normalised by the inlet gas concentration as in case of removal efficiency and molar flux.

Whilst concentration gradient strongly influences methane permeability through the PDMS membrane, liquid ambient temperatures are likely to affect the response of the PDMS material with respect to methane fluxes and recoveries. In this study, the recorded process temperatures at the lowest V_L in vacuum operation were up to 8 °C lower than the temperatures observed in sweep gas mode (Table 21). Such high temperature gradient has a significant impact on gas permeability through the PDMS membrane. For instance, *Raharjo et al. (2007)* reported methane permeability of 1200 Barrers at 25 °C; 10 °C rise in the temperature increased methane permeability through PDMS by *c.* 8%. Similar methane behaviour in PDMS films was reported by *Pinnau and He (2004)*.

Table 21. Example process temperatures on the inlet and outlet of the PDMS membrane module in sweep gas and vacuum operation.

Stripping medium	V_L	T_{IN}	T_{OUT}	Season
	$(m.s^{-1})$	(°C)	(°C)	
Sweep gas	0.00036	19	17	Autumn
	0.0242	19	18	Autumn
	0.0472	19	19	Autumn
Vacuum	0.00017	19	9	Winter
	0.0242	19	13	Winter
	0.0472	19	19	Winter

Based on the hydrodynamic conditions tested, steady-state was reached between 1 minute (lowest V_L) and 86 minutes (highest V_L), equivalent to *Re* 1.3 and 344, respectively. In the winter season, an increase in hydraulic retention time (*i.e.* at the lowest V_L) resulted in a significant liquid temperature drop of 10 °C at the outlet of the membrane module. In contrast, in warmer seasons liquid outlet temperatures differed by max. 2 °C between the lowest and highest V_L. High liquid outlet temperatures positively affected process efficiency, consequently greater methane recoveries at the highest liquid velocities were observed. To demonstrate, at constant CH_4 inlet concentrations of 28.33 mg.L^{-1} (SD ±1.16) and average outlet temperatures of 18 °C (±1) in sweep gas operation CH_4 recoveries were proportional to the decrease in liquid velocity. When employing vacuum, liquid ambient temperatures at the highest V_L were 6 °C greater than the temperatures at the intermediate V_L of 0.0242 m.s^{-1}; consequently *c.* 66% increase in CH_4 removal efficiency in comparison with moderate liquid velocity was observed.

Overall, the observed trends indicate that methane recovery increases with decreasing liquid hydrodynamics and strongly depends on methane concentrations in the inlet stream and liquid ambient temperatures.

It is worth noting that in the liquid de-gassing processes the lumen feed operation mode is often preferred over the shell feed (*Tan et al., 2005*). In the shell side feed, distribution of fluid along the fibres broadens the residence time of the fluid particles, enhanced at low liquid velocities. At high liquid velocities, mass transfer is enhanced due to the shorter residence time of the fluid particles at the boundary layer (*i.e.* increase in concentration driving force). This effect is even more noticeable for low fibre packing densities ϕ (ϕ 3-40%). The mass transfer coefficients increase with greater packing densities until the values of ϕ 65-70% are obtained. Further increase in ϕ results in the formation of 'dead zones' between the closely packed fibres and consequently lower mass transfer coefficients are obtained. By introducing the liquid into the lumen these undesired phenomena are diminished (*Stanojevic et al., 2003*). In this study, however, the shell-feed was employed due to the possibility of lumen blockage by suspended solids.

4.1.2 The Effect of Gas Hydrodynamic Conditions on Pure Methane Recovery

In a second step, a series of experiments enabling the estimation of the stripping medium effect (*i.e.* nitrogen sweep gas or vacuum) on methane recovery was undertaken. The effect of sweep gas velocity was evaluated over the range 0.033 - 2.39 m.s^{-1} (*Re* 7.3 - 529) at a constant liquid velocity of 0.0061 m.s^{-1} (*Re* 44). Methane recovery remained unchanged at a relatively consistent 36% methane removal, equivalent to 18.5 mg.L^{-1} (SD $\pm$0.9) CH$_4$ outlet concentrations (Figure 26a and b). The observed methane fluxes through the PDMS membrane also remained independent of sweep gas velocity (Figure 26c). The independence of transfer as a function of gas velocity indicates that mass transfer is not governed by the gaseous phase boundary layer, which has been reported previously for other partially soluble gases (*Tan et al., 2005*).

This observation can be explained by the low partial pressure of methane in the nitrogen sweep gas; the highly dilute permeate stream maintains the concentration gradient such that gas mass transfer resistance is negligible.

Alternatively, sweep gas operation may be replaced by vacuum operation (Figure 26d, e, f). In this study, a low applied vacuum pressure, P_{VAC}, < 15 mBar has been demonstrated to achieve > 76% methane recovery under an intermediate liquid velocity of *c.* 0.0061 m.s^{-1} (*Re* 44). At the lowest (most efficient) liquid velocity of 0.00036 m.s^{-1} (*Re* 2.6) and P_{VAC} < 15 mBar, the recorded methane extraction efficiencies exceeded 88%. The application of the lowest V_L positively affected dissolved methane recovery and indicates that soluble gas permeation through PDMS membrane is controlled by both dynamics: vacuum pressure and liquid velocity.
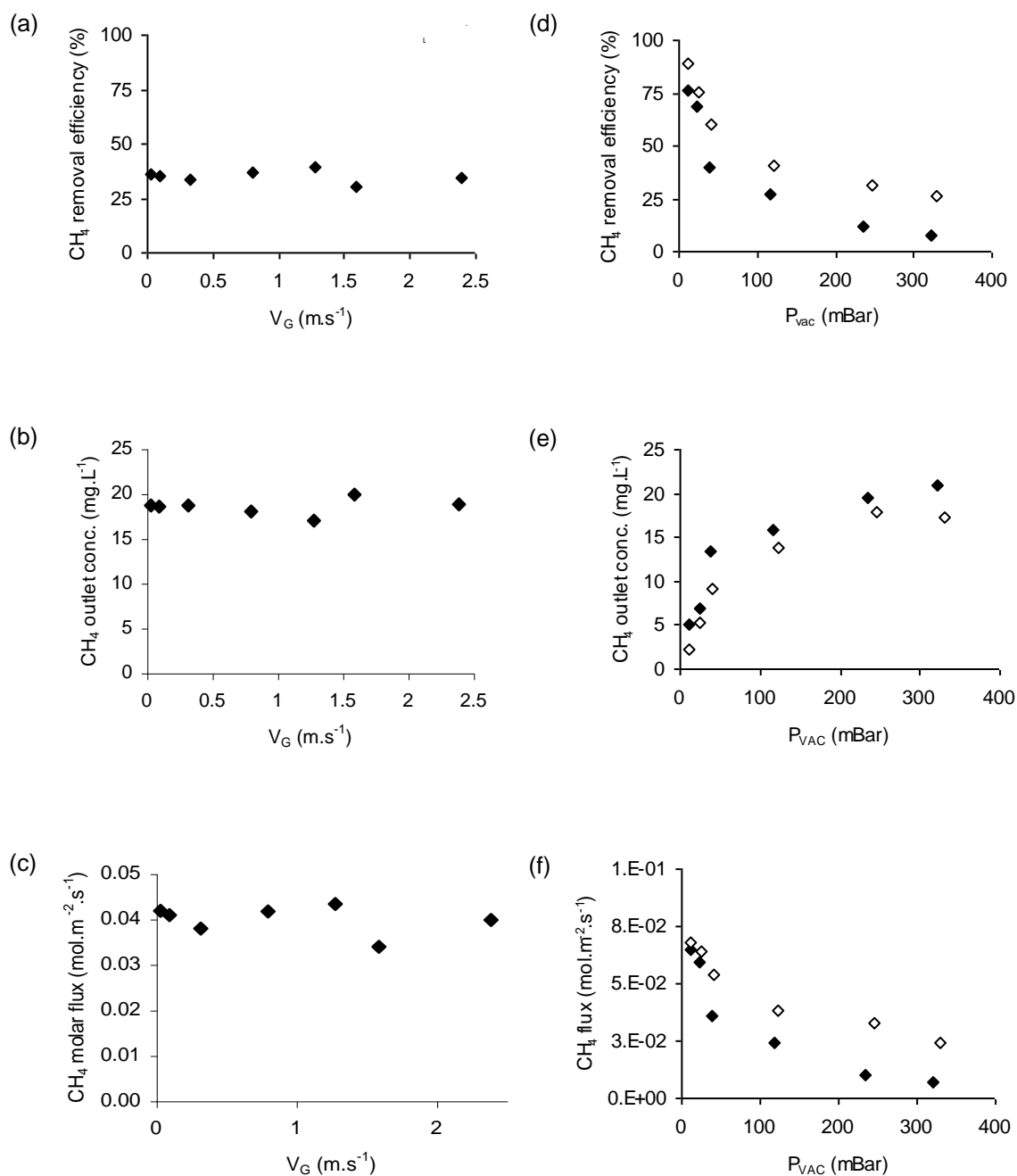
Figure 26. Effect of gas hydrodynamic conditions on pure methane recovery in a shell-feed operational mode. Sweep gas, V_G = 0.033 m.s^{-1}: (a) CH_4 removal efficiency; (b) CH_4 outlet concentration; (c) CH_4 molar flux. Vacuum, P_{vac} = 24 mBar: (d) CH_4 removal efficiency; (e) CH_4 outlet concentration; (f) CH_4 molar flux. ♦ V_L = 0.0061 m.s^{-1}; ◊ V_L = 0.00036 m.s^{-1}. Removal efficiency is defined as follows: $(((c_{IN}-c_{OUT})/c_{IN})*100\%)$; where c_{IN} is the gas inlet concentration (mg.L^{-1}); c_{OUT} is the gas outlet concentration (mg.L^{-1}).

4.1.3 Dissolved Gases Recovery from Binary CH_4/CO_2 Mixtures

Whilst this study introduces the concept of dissolved methane recovery from liquids, carbon dioxide is also present as a principal component of the headspace gas. Due to high CO_2 solubility in liquids (*i.e.* CO_2 is *c.* 75 times more soluble in water than CH_4), CO_2 losses in the liquid phase are significant. To evaluate the impact of carbon dioxide presence on methane recovery, water saturated with a binary CH_4/CO_2 mixture within the concentration range from 25 to 75 vol.% CH_4 in balance with CO_2 was employed as a synthetic solution. Liquid containing dissolved gases passed through the shell side of the membrane module at velocities ranging from 0.00036 to 0.0472 m.s^{-1} (*Re* 2.6 - 344), whilst sweep gas (Figure 27a, b, c) or vacuum (Figure 27d, e, f) introduced counter-currently enabled dissolved gases recovery. In both operational modes an increase in CO_2 concentration in the feed mixture generally resulted in greater CH_4 recoveries. To illustrate, when employing 75:25 vol.% CH_4:CO_2 binary mixture under vacuum operation at the lowest V_L, the recorded CH_4 removal efficiency reached the value of 72.2% and increased to 81.2% and 84.9% when 50:50 vol.% and 25:75 vol.% CH_4:CO_2 mixture was employed, respectively (Figure 27d). The effect was further intensified at intermediate and high liquid velocities, *i.e.* V_L > 0.0242 m.s^{-1} (*Re* > 176). For instance, CH_4 removal efficiency significantly increased by 64% when employing 25:75 vol.% CH_4:CO_2 mixture in comparison with removal efficiency obtained for pure CH_4 (equivalent to 91% decrease of CH_4 concentration in the retentate stream). However, in terms of CH_4 molar fluxes, an increase in CO_2 concentration in the feed solution resulted in considerably lower methane fluxes. To demonstrate, the obtained molar flux values for pure CH_4 solution at highest V_L reached 0.48 mol.m^{-2}.s^{-1}; when employing 25:75 CH_4:CO_2 mixture CH_4 molar flux decreased by 99% (Figure 27f). This indicates that methane permeability through the PDMS is governed by concentration gradient across the membrane.

Figure 27. Effect of liquid velocity on methane recovery in pure and binary systems. Sweep gas, V_G = 0.033 m.s^{-1}: (a) CH$_4$ removal efficiencies; (b) CH$_4$ outlet concentrations; (c) CH$_4$ molar fluxes. Vacuum, P_{vac} = 24 mBar: (d) CH$_4$ removal efficiencies; (e) CH$_4$ outlet concentrations; (f) CH$_4$ molar fluxes. ◆100 vol.% CH$_4$; ◇75:25 vol.% CH$_4$:CO$_2$; △50:50 vol.% CH$_4$:CO$_2$; ×25:75 vol.% CH$_4$:CO$_2$. Removal efficiency is defined as before.

Employing 25 - 100 vol.% CO_2 mixtures in balance with methane enabled the estimation of CO_2 permeation behaviour when present in binary CO_2/CH_4 mixtures. The operational conditions (*i.e.* V_L, V_G, P_{vac}) were the same as reported above for CH_4/CO_2 binary systems. As expected, maximum CO_2 recoveries in pure systems were recorded at lowest liquid velocities and reached the value of *c.* 64% and 31% for sweep gas and vacuum operation, respectively (Figure 28a and d); equivalent to 0.7 (SD ±0.17) $g.L^{-1}$ and 1.0 (SD ±0.04) $g.L^{-1}$ CO_2 as the outlet concentrations. The same effect was observed when introducing binary mixtures, *i.e.* CO_2 recoveries were found to decrease up to 98% of the initial value with an increase in liquid velocity. When increasing the amount of dissolved methane in the feed stream, CO_2 outlet concentrations were found to decrease (Figure 28b and e). To illustrate, when present as 75:25 vol.% CO_2:CH_4 mixture under sweep gas operation, CO_2 outlet concentration reached 0.77 (SD ±0.31) $g.L^{-1}$. In contrast, when 25:75 CO_2:CH_4 vol.% solution was employed, the recorded CO_2 outlet concentration was 0.45 (SD ±0.04) gL^{-1}.

It is worth noting that at high V_L > 0.045 $m.s^{-1}$ (*Re* > 328) in vacuum mode, pure CO_2 molar flux was up to 56% lower in comparison with CO_2 molar fluxes obtained for model binary CO_2:CH_4 mixtures (Figure 28f). This observation can be explained by previously discussed process dependency on liquid ambient temperatures and inlet gas concentrations. The obtained results indicate that the CO_2 recovery process is a function of developed CO_2 gradient concentration across the membrane wall and dissolved methane do not influence CO_2 permeability through PDMS membrane.
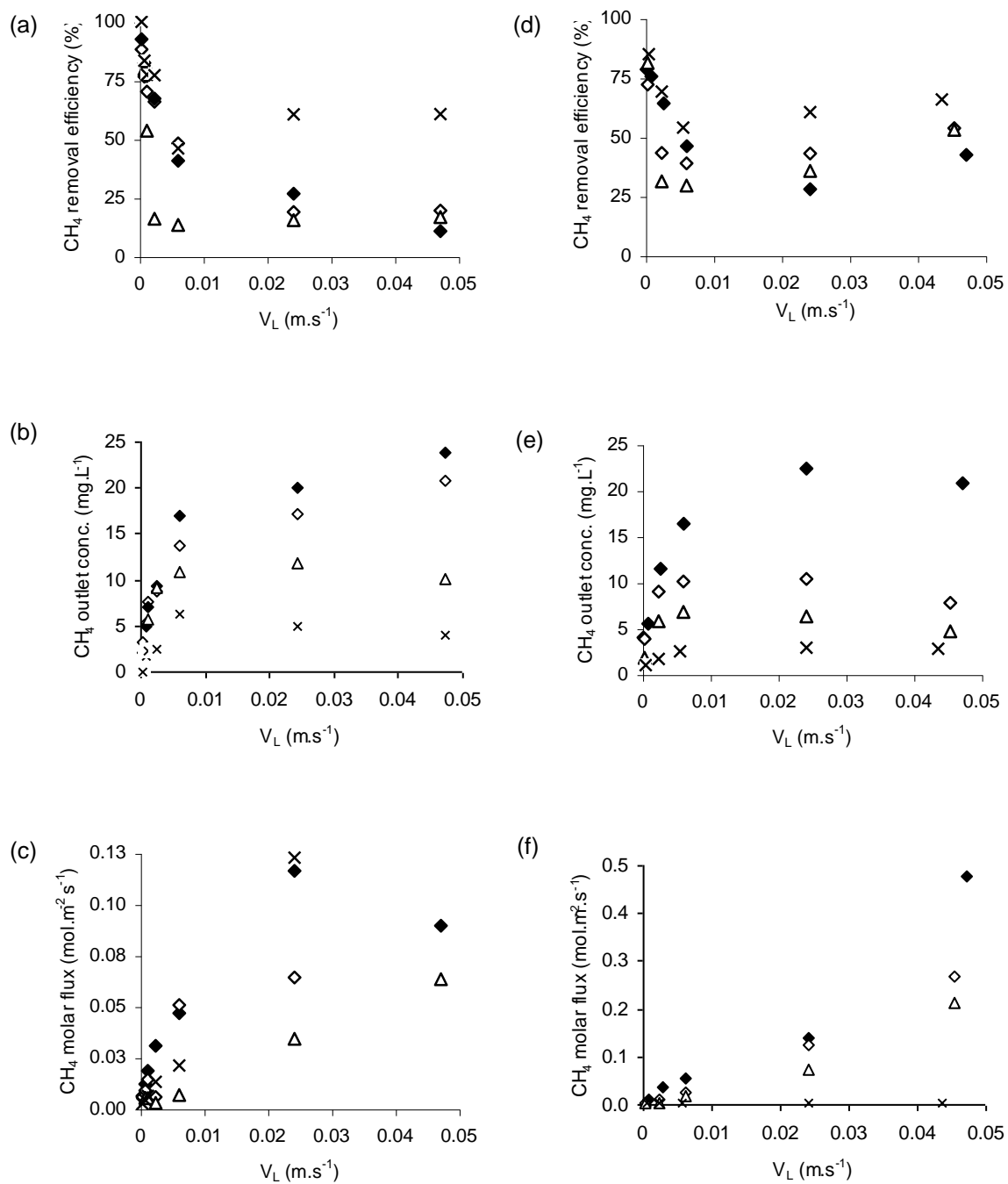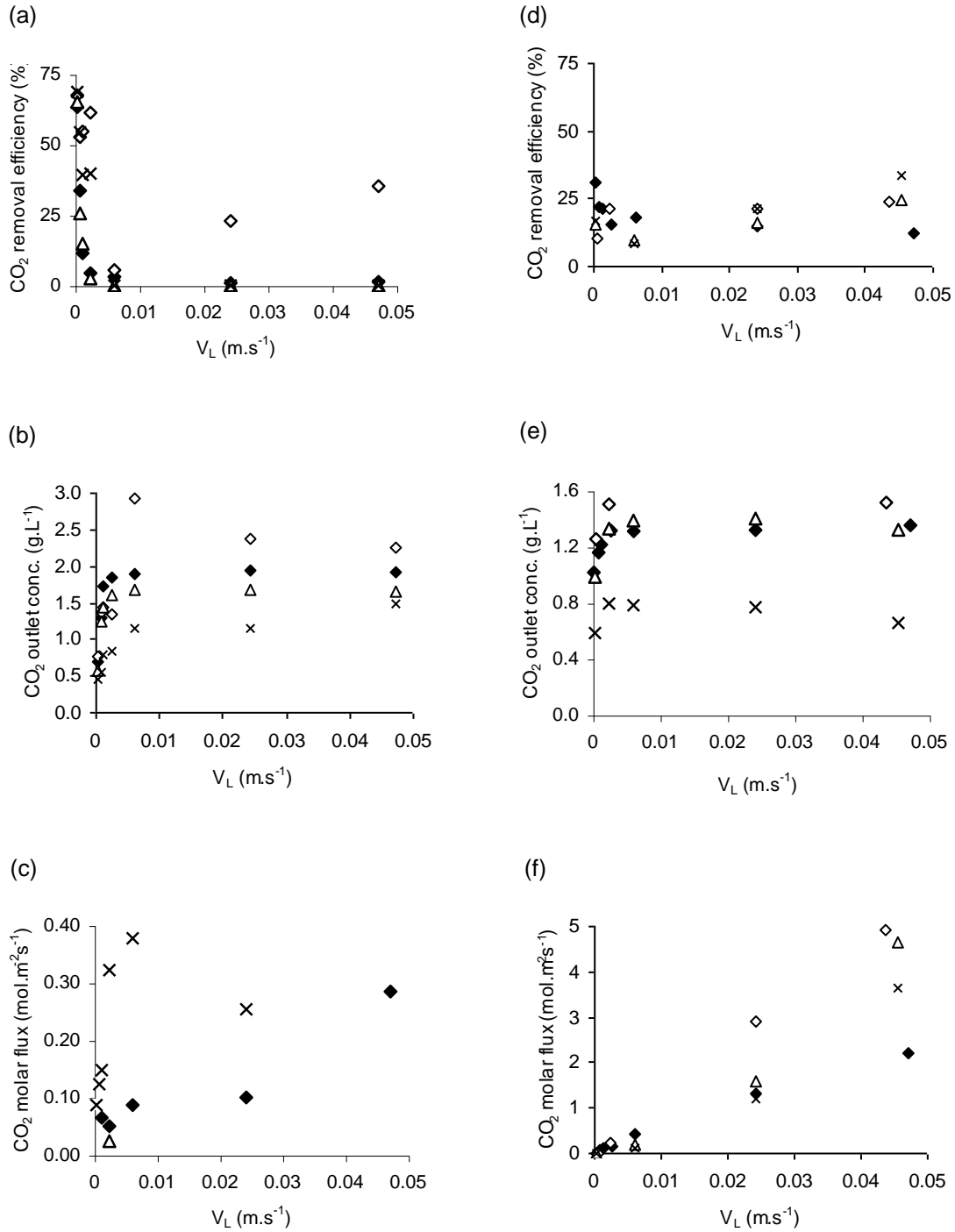
Figure 28. Effect of liquid velocity on carbon dioxide recovery in pure and binary systems. Sweep gas, V_G = 0.033 m.s^{-1}: (a) CO_2 removal efficiencies; (b) CO_2 outlet concentrations; (c) CO_2 molar fluxes. Vacuum, P_{vac} = 24 mBar: (d) CO_2 removal efficiencies; (e) CO_2 outlet concentrations; (f) CO_2 molar fluxes. ◆100 vol.% CO_2; ◇75:25 vol.% CO_2:CH_4; △50:50 vol.% CO_2:CH_4; ×25:75 vol.% CO_2:CH_4. Removal efficiency is defined as before.

4.1.4 The Effect of Membrane Wall Thickness on Dissolved Methane Recovery

To determine the impact of PDMS membrane wall thickness (t_m) on dissolved methane recovery, two synthetic modules of comparable contact area of 0.094 m^2 (SD ±0.0007) were employed: *Module 1* with t_m of 0.25 mm and *Module 2* with t_m of 1.0 mm. Since sweep gas hydrodynamics do not affect methane extraction efficiency, nitrogen sweep velocities were kept constant at V_G of 0.033 $m.s^{-1}$ (*Re* 53), whilst liquid velocities ranged from 0.00036 $m.s^{-1}$ to 0.0472 $m.s^{-1}$ (*Re* 2.6 to 439). When utilising *Module 1*, recorded process efficiencies under the lowest (most efficient) V_L reached 93%, equivalent to 2.1 (SD ±0.06) $mg.L^{-1}$ as an outlet CH_4 concentration. In contrast, employing *Module 2* the obtained CH_4 removal efficiency decreased to 87%, equivalent to 2.9 (SD ±0.07) $mg.L^{-1}$ of CH_4 in the retentate stream (Figure 29a and b). The effect was further increased at liquid velocities exceeding 0.0024 $m.s^{-1}$ (*Re* 20), *i.e.* when employing *Module 2* methane recoveries decreased by *c.* 79% in comparison with the recoveries obtained for *Module 1*. In terms of CH_4 molar fluxes, significantly higher values were recorded for *Module 1*. For instance, at intermediate and high V_L (*Re* 176 - 439), CH_4 molar fluxes were 0.12 $mol.m^{-2}.s^{-1}$ and 0.02 $mol.m^{-2}.s^{-1}$ for module *Module 1* and *Module 2*, respectively (Figure 29c).
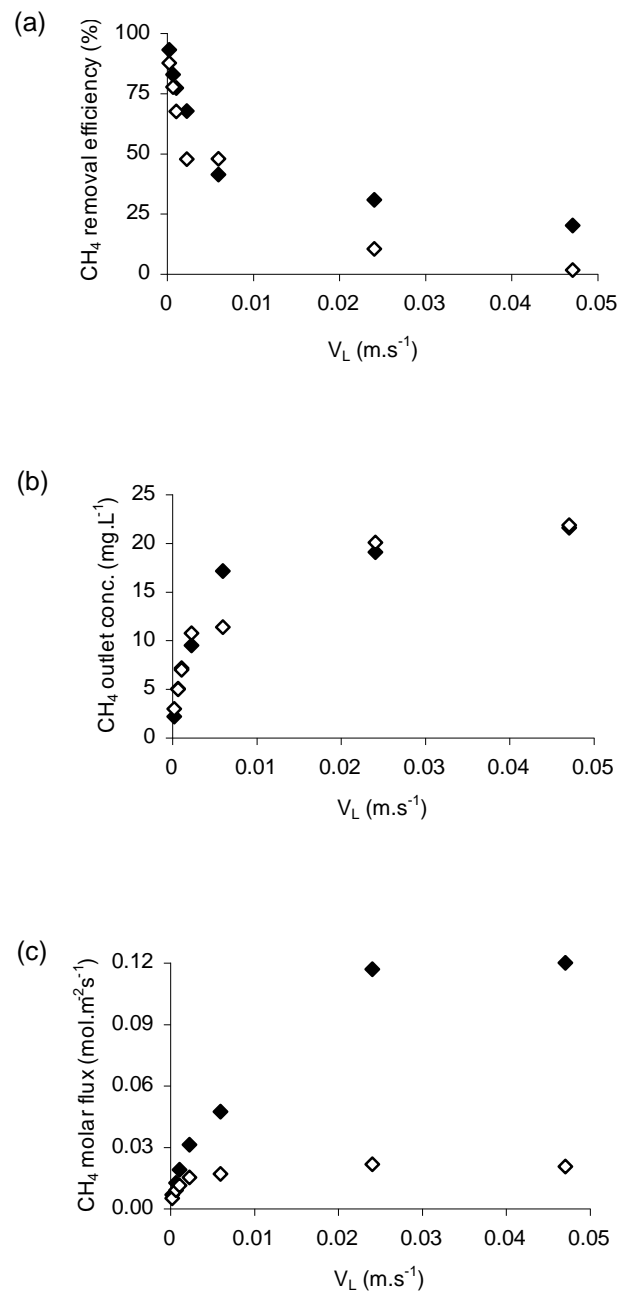
Figure 29. Pure methane recovery from water as function of liquid velocity for thin and thick wall de-gassing membrane modules: (a) methane removal efficiency; (b) methane outlet concentrations; (c) methane molar flux. ♦ tm = 0.25 mm; ◊ tm = 1.0 mm; V_G = 0.033 m.s^{-1}. Removal efficiency is defined as before..

The effect of membrane wall thickness on the overall mass transfer was determined using the Wilson plot approach (Eq. 8). The overall mass transfer

resistance ($1/K_{ov}$) was experimentally obtained from CH_4 mass flux (Eq. 9) and plotted against $V_L^{-0.33}$ (Figure 30a and b).
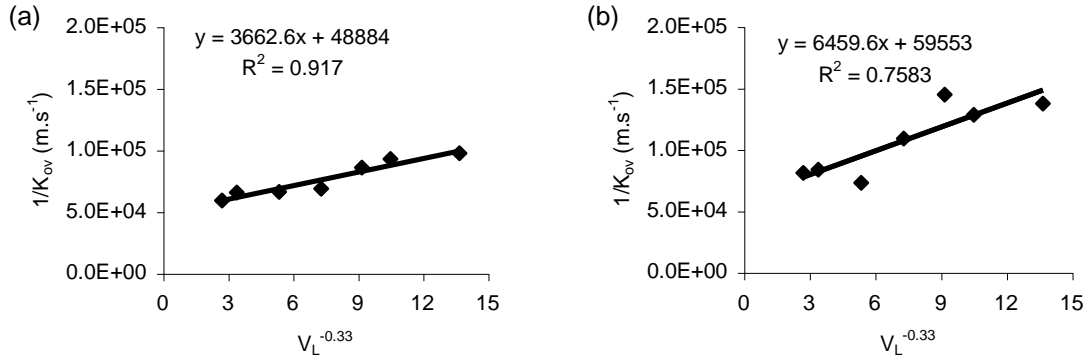
Figure 30. Wilson plot for pure methane - nitrogen sweep system: (a) ♦ tm = 0.25 mm; (b) ◊ tm = 1.0 mm. V_G = 0.033 m.s^{-1}.

Membrane resistance obtained for *Module 2* with t_m of 1.0 mm was 18% greater in comparison with the resistance obtained for *Module 1* with t_m of 0.25 mm. *Doig et al. (1999)* similarly observed up to 70% decline in $1/K_{ov}$ when membrane thickness increased from 0.25 mm to 1.0 mm, whilst extracting solutes from organic solvents using silicone rubber. This indicates that the thickness of the membrane wall limits methane diffusion through the PDMS material. Because of increased membrane resistance (proportional to an increase in membrane thickness), diffusivity of methane through the PDMS membrane decreases due to increased distance the diffusing methane molecule has to pass through. The overall mass transfer coefficients at the lowest V_L (*Re* 2.6) were 1.03 E-05 m.s^{-1} for t_m of 0.25 mm and 7.29 E-06 m.s^{-1} for t_m of 1.0 mm. In contrast, K_{ov} values at highest V_L (*Re* 344 and 439 for *Module 1* and *Module 2*, respectively) increased by *c.* 63% and *c.* 70%. Significantly greater K_{ov} values at higher Reynold's numbers were also reported by *Cocchini et al. (2002)*; to illustrate, increasing *Re* from 565 to 3565 corresponded to *c.* 60% increase in K_{ov} (equivalent to 3.35 E-05 m.s^{-1}). Critical liquid velocity, above which mass transfer across the membrane had no significant effect on the overall mass transfer coefficient, was estimated at 0.0061 m.s^{-1}, equivalent to *Re* 44 (Figure 31).
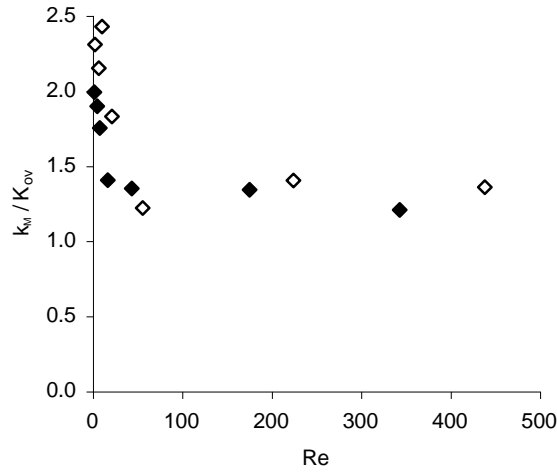
Figure 31. Relative mass transfer coefficient in pure methane – nitrogen sweep system as a function of Reynold's number. ♦ $tm = 0.25$ mm; (b) ◊ $tm = 1.0$ mm. $V_G = 0.033$ m.s^{-1}.

4.1.4.1 Determination of Liquid Phase Mass Transfer Resistance

The effect of sweep gas phase on the overall mass transfer is negligible; thus the impact of V_L on liquid phase mass transfer resistance ($1/k_L$) can be estimated from $1/K_{ov}$ and previously determined membrane resistance; therefore overall mass transfer resistance is given by:

$$\frac{1}{K_{ov}} = \frac{1}{k_L} + \frac{1}{k_M m}$$

(Eq.18)

In both modules liquid phase resistance decreased with increasing liquid hydrodynamics (Figure 32). To demonstrate, the obtained $1/k_L$ at V_L of 0.00036 m.s^{-1} was 48200 s.m^{-1}, contributing to 50% of the overall mass transfer resistance; increasing V_L to 0.0472 m.s^{-1} reduced $1/k_L$ to 9940 s.m^{-1} and contributed to 17% of the overall resistance (t_m of 0.25 mm). For module with t_m of 1.0 mm and $V_L < 0.0061$ m.s^{-1} liquid phase mass transfer resistance significantly increased by up to 62% in comparison with t_m of 0.25 mm; consequently contributing to 57% of the $1/K_{ov}$. *Cocchini et al. (2002)* similarly observed greater $1/k_L$ at lowest liquid velocities as a result of increased thickness of liquid phase boundary layer.
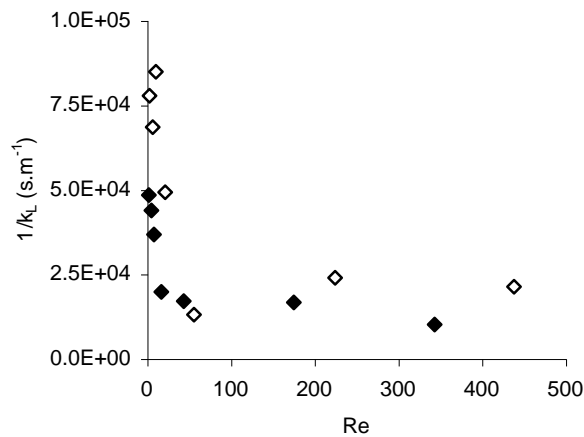
Figure 32. Liquid phase mass transfer resistance as a function of Reynold's number. ♦ $tm = 0.25$ mm; (b) ◊ $tm = 1.0$ mm. $V_G = 0.033$ m.s^{-1}.

4.1.5 Sherwood Number Correlations

To evaluate the impact of liquid hydrodynamics on Sherwood number (expressing overall mass transfer coefficient) liquid saturated with CH_4 was introduced into the shell of the *Module 1*; vacuum was employed counter-currently at P_{vac} of 24 mBar. At the lowest liquid *Re* of 1.3 experimentally obtained K_{ov} was 1.82 E-06 m.s^{-1} (equivalent to *Sh* of 7.4); in contrast, at the highest *Re* of 344 K_{ov} values of 102 E-06 m.s^{-1} were achieved (*Sh* 335). Experimental data were compared with the correlations obtained from the literature (see Table 17; section *2.2.4.1*). The results obtained in this study fit between models developed by *Crowder and Cussler (1998)* and *Tan et al. (2005);* (Figure 33). The non-linearity of the experimentally obtained data is a result of the strong influence of the liquid ambient temperatures on Schmidt number. *Sc* number is a function of physical properties of the liquid and the diffusivity of the gas in the liquid that strongly depends on the temperature. To demonstrate, *Sc* at 9 °C was 556; 8 °C increase in the water temperature resulted in 22% decrease in *Sc* number. Based on this conclusion, it can be assumed that the correlation developed by *Crowder and Cussler (1998)* enables the closest prediction of the experimental data.
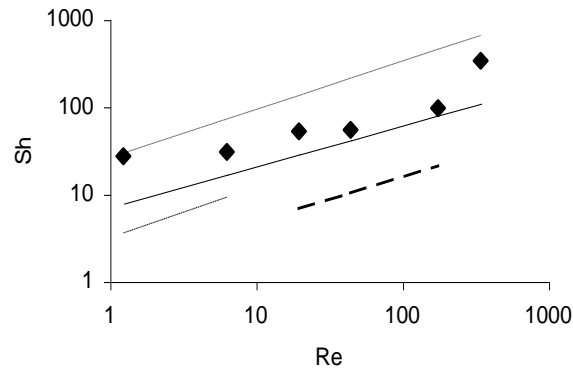
Figure 33. Sherwood number as a function of Reynold's number on a log-log scale for shell feed operation; P_{vac} = 24 mBar. - - - - *Costello et al. (1993)*; —— *Crowder and Cussler (1998)*; - · - · - *Ferreira et al. (1998)*; ·········· *Tan et al. (2005).*

4.2 Methane Recovery from Low Temperature Anaerobic Effluent

4.2.1 Methane Loss in Anaerobic Effluent

Removal of COD within the Expanded Granular Sludge Blanket (EGSB) reactor averaged 64 ±9% (*n* = 15) for the period studied. A methane gas flow rate of *c.* 4.6 L.d^{-1} was recorded which resulted in a methane yield of *c.* 0.21 L.gCOD^{-1}. This result is in agreement with the low temperature study of *Uemura and Harada (2000)* that reported a yield of 0.23 L.gCOD^{-1}. The yields reported are below the theoretical ratio of 0.35 L.gCOD^{-1} (*Tchobanoglous et al., 2003*) and can be directly attributed to the raised solubility state of methane gas at low operating temperatures.

An average dissolved methane concentration of 25.4 mg.L^{-1} was recorded in the effluent. For comparison, according to Henry's law, the predicted dissolved methane concentration at the effluent temperature of 16 °C is 21.9 mg.L^{-1}. This disparity between measured and predicted results indicates methane supersaturation of the anaerobic effluent by a factor of 1.57. *Hartley and Lant (2006)* recently summarised data from a number of anaerobic studies (Table 22) and established supersaturation factors of between 3.8 and 6.9. The

77

significance of this result is that on average, *c.* 45% of the produced methane exits the reactors in the effluent.

Based on the biogas methane fraction, a potential net electrical production of +0.14 $kWh_e.m^{-3}$ treated effluent is achievable (after accounting for the parasitic electrical demand based on 32% electrical efficiency), demonstrating that the EGSB is energy positive. The resultant carbon reduction is therefore estimated as +0.06 $kg.m^{-3}$ based on a release of 0.43 $kg.kWh^{-1}$ of grid electricity (*DEFRA, 2007*). However, using the global warming potential (GWP) factor for methane (*IPCC, 2007*), the fugitive methane emission accounts for a carbon equivalent emission of -0.53 $kg.m^{-3}$ indicating that at this operating temperature, without recovery of the dissolved methane, the EGSB is currently carbon negative.

Table 22. Methane mass balances from several low temperature anaerobic pilot studies.

	Total CH$_4$ production				
Average temperature	Biogas	Effluent	Average CH$_4$ loss in the effluent	Degree of supersaturation	Reference
(°C)	(g.d^{-1})	(g.d^{-1})	(%)	(-)	
29	0.3	1.6[a,b]	85	3.8[a]	*Noyola et al. (1988)*
18	16.7	62.3[a,b]	79	5.0[a]	*Barbosa and Sant' Anna (1989)*
28	12.9	72.0[a,b]	85	6.9[a]	*Singh et al. (1996)*
16	0.34-2.1	0.27-1.36[a,b]	39	-	*Uemura and Harada (2000)*
16 (±1)	3.1	2.8 (±0.9)	45 (±8.5)	1.57	This study

[a]Data collated from *Hartley and Lant, 2006.* [b]Losses calculated theoretically using COD mass balance.

4.2.2 Dissolved Methane Recovery

The EGSB effluent passed from the reactor separator into a buffering storage tank prior to discharge to drain. During this brief transition, the dissolved methane concentration reduced from 25.4 mg.L^{-1} to 12.2 ($\pm$7) mg.L^{-1}. Effluent from the buffering tank was pumped into the shell side of the *Module 3*. During the first set of experiments, gas velocity was maintained constant at 0.175 m.s^{-1} (*Re* 37) and liquid velocity varied between 0.0033 m.s^{-1} (*Re* 47) to 0.064 m.s^{-1} (*Re* 886). The highest efficiency of 72% was recorded at the lowest liquid velocity (Figure 34a). With increasing liquid velocity, methane recovery efficiency decreased to 9.5% (*c.* 87% of the initial value).
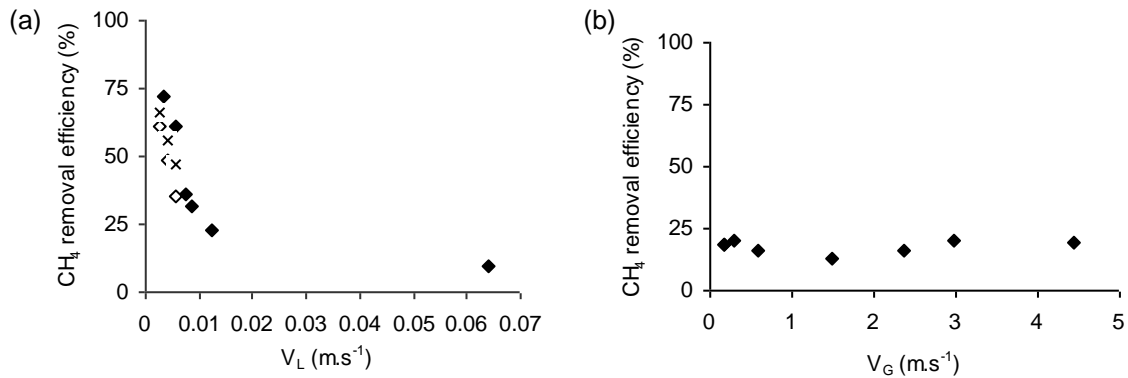
Figure 34. Methane removal efficiency as a function of: (a) liquid velocity, V_G = 0.175 m.s^{-1}; (b) sweep gas velocity, V_L = 0.0125 m.s^{-1}. Effluent containing 95:5 vol. % CH_4:CO_2. ♦ run 1; ◊ run 2; × run 3.

The effect of sweep gas velocity was evaluated using gas velocities ranging from 0.125 m.s^{-1} (*Re* 26) to 3.11 m.s^{-1} (*Re* 651) at a constant liquid velocity of 0.0125 m.s^{-1} (*Re* 173). Methane recovery remained practically unchanged at a relatively consistent *c.* 20% methane removal (Figure 34b). The observed trends are consistent with the results obtained for the synthetic experiments: (i) mass transfer is controlled by liquid hydrodynamics; (ii) independence of methane transport from gas velocity indicates that mass transfer is not governed by gas phase boundary layer.

Based on the optimum conditions determined in this study (influent 12.2 mg.L^{-1} of CH$_4$, 72% recovery), the net electrical output achieved by the EGSB could increase from +0.14 kWh$_e$.m^{-3} to +0.183 kWh$_e$.m^{-3}. In addition, the resultant carbon balance for electrical production (CO$_{2e}$) and fugitive emissions are +0.08 kg.m^{-3} and -0.07 kg.m^{-3} respectively and indicate that by integrating methane recovery, treatment of domestic wastewater using low temperature EGSB processes can become carbon positive. In practice, an increase in the proportion of electrical energy produced from recovered methane is anticipated, since the losses in this study between the separator and the buffer tank of *c.* 52% were not accounted for. Using these data and the same recovery factor, electrical output will increase to +0.229 kWh$_e$.m^{-3}, yielding a further positive carbon return of +0.1 kg.m^{-3} (*net* +0.03 kg.m^{-3}).

4.2.3 Downstream Gas Quality and Re-use

At the lowest liquid velocity of 0.0033 m.s^{-1} (highest process efficiency), CH$_4$ mass flux of 0.35 mg.min^{-1} was observed. At the applied nitrogen sweep gas flow rate (Q_G) of 0.85 L.min^{-1}, the purity of the recovered methane in the gas phase was *c.* 0.06 vol.% (Figure 35). At the highest liquid velocity, whilst lower methane recovery was achieved, a higher CH$_4$ flux of 2.34 mg.min^{-1} was observed; equivalent to 0.41 vol.% of methane in the permeate stream (Figure 36).
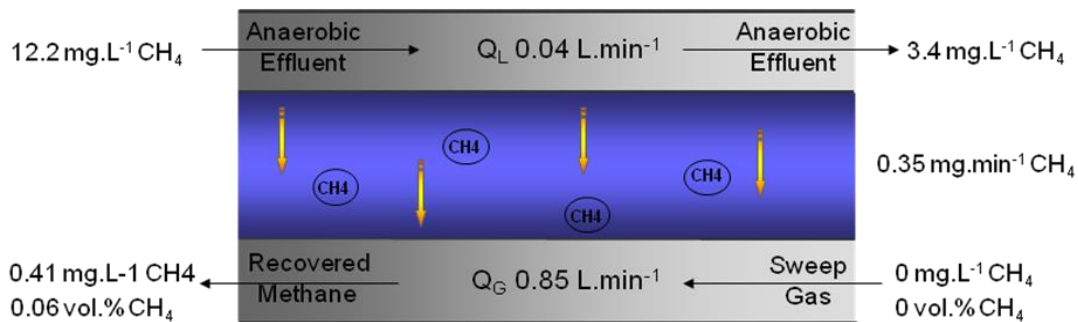
Figure 35. Methane mass balance across PDMS membrane for the lowest V_L of 0.0033 m.s^{-1} (Q_L= 0.04 L.min^{-1}); V_G = 0.175 m.s^{-1} (Q_G= 0.85 L.min^{-1}).
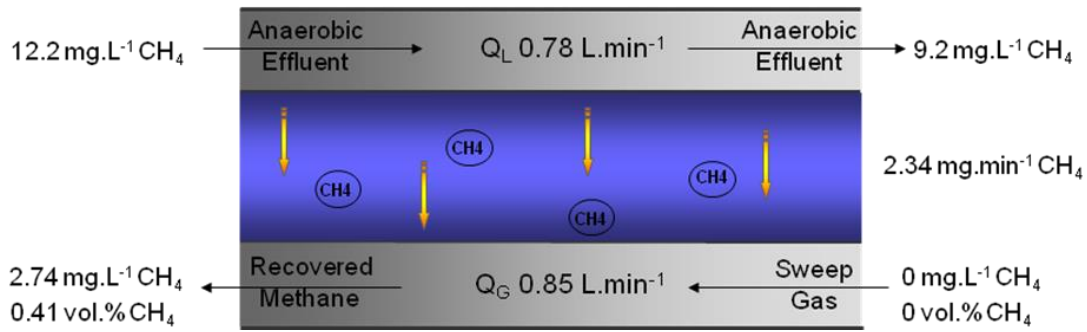
Figure 36. Methane mass balance across PDMS membrane for the highest V_L of 0.064 m.s^{-1} (Q_L= 0.78 L.min^{-1}); V_G = 0.175 m.s^{-1} (Q_G= 0.85 L.min^{-1}).

Alternatively, sweep gas operation may be replaced by vacuum operation (Figure 37). In this study, low applied vacuum pressure, P_{VAC}, < 20 mBar have been demonstrated to achieve reasonable methane recovery of 55% at an intermediate liquid velocity of *c.* 0.0056 m.s^{-1} (*Re* 91). In contrast, maintaining the identical liquid hydrodynamics and temperatures, sweep gas operation resulted in *c.* 25% lower methane removal efficiency. *Tan et al. (2005)* similarly reported *c.* 33% lower oxygen removal in sweep gas mode when utilising silicone membranes.
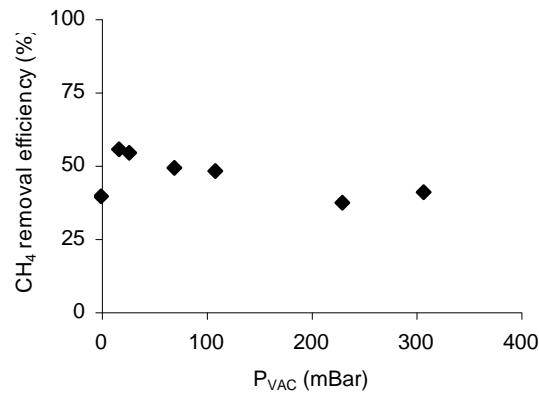
Figure 37. Methane removal efficiency as a function of vacuum pressure; V_L = 0.0056 m.s^{-1}. Effluent containing 95:5 vol.% CH_4:CO_2.

Whilst the comparative parasitic energy demand of the two operational modes requires further investigation, vacuum mode offers the potential to deliver much higher recovered gas purities (*Vallieres and Favre, 2004*). However, in this study, CH_4 content in the permeate stream was only 0.004

vol.%; equivalent to 0.46 mg.min^{-1} CH$_4$ mass flux (Figure 38). Highly diluted permeate stream, when operating in the vacuum mode, is a result of: (i) low applied liquid velocities and; (ii) relatively high vacuum flow rate.
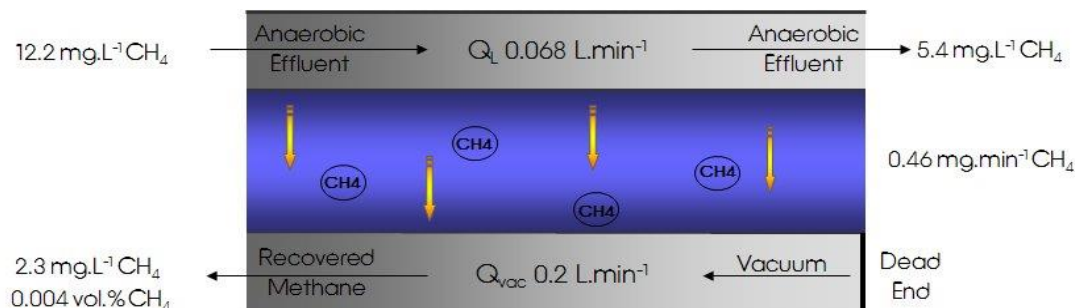
Figure 38. Methane mass balance across PDMS membrane for the most-efficient vacuum pressure of P_{vac} = 14 mBar (Q_{vac}= 0.2 L.min^{-1}); V_L = 0.0056 m.s^{-1} (Q_L= 0.068 L.min^{-1}).

To increase the suitability of the gas phase for re-use, the methane permeate stream must be highly concentrated. Rate limiting conditions need to be established to further maximise gas quality and minimise the impact of gas mass transfer; this may be achieved by: (i) recirculation of the sweep gas/vacuum or; (ii) reducing gas flow rate to increase gas purity. In the first case, the installation would require re-design and an additional pump would add to the overall operational cost. In the latter case, when lowering gas flow rate to Q_G of 0.01 L.min^{-1} at liquid flow rate of 0.78 L.min^{-1}, methane content in the permeate stream would increase to 26 vol.%. To compare, when operating at Q_G of 0.85 L.min^{-1}, the recorded methane content was 0.41 vol.%. However, it would be necessary to determine the impact of gas phase mass transfer resistance on the process efficiency when operating at very low Q_G.

4.3 Maximising Methane Recovery

Highest methane efficiency recoveries were obtained at the lowest liquid velocities < 0.00036 m.s^{-1} (*Re* < 2.6). A critical liquid velocity, above which process efficiencies decreased significantly, was established at V_L of 0.0024 m.s^{-1} (*Re* 18). Although low liquid velocities favour dissolved methane recovery, high liquid velocities offer a potential to deliver much higher methane fluxes per minute of operation. However, to maintain efficient performance at high V_L,

significant amounts of methane exiting the system have to be reduced. One pragmatic solution may be to configure PDMS contactors in series; this would permit high methane fluxes and similar overall recoveries, provided the number of contactors required could be optimised. Assuming consistent recovery, the additional number of membrane contactors minimises the amount of dissolved methane exiting the system in the retentate stream. To illustrate, when theoretically employing three contactors in series, at the lowest V_L of 0.00036 m.s^{-1}, the achieved overall CH$_4$ recovery could be as high as 99.97%; equivalent to 0.01 mg.L^{-1} of CH$_4$ in the retentate stream (Figure 39).

Figure 39. Methane outlet concentrations for PDMS modules in series assuming *c.* 93% removal efficiency for every contactor; V_L of 0.00036 m.s^{-1}.

For intermediate liquid velocities of 0.0061 m.s^{-1}, reasonable overall methane recovery of 76% was possible, equivalent to 6.7 mg.L^{-1} of CH$_4$ in the exiting liquid stream. To achieve the same recoveries at highest V_L, (*i.e.* highest methane fluxes) the number of the employed contactors would have to be significantly increased to +10. Another suggestion is to significantly increase membrane contact area and module packing density. This can be done by employing greater number of PDMS hollow fibres of thinner inner diameter and membrane wall. This would provide much larger membrane surface for methane to dissolve in and diffuse through PDMS fibres.

Based on the maximum recovery achieved in this study (93%) and assuming no methane losses during the transition from reactor separator to the storage tank, recovery of 3.5 L.day^{-1} of CH$_4$ from anaerobic liquid is possible. Recovered CH$_4$ can be then directed to the biogas stream and upgraded to natural gas standards via porous hollow fibre membrane contactors. Assuming +95% absorption efficiency (*Bottino et al., 2006*; *Mavroudi et al., 2003*; *Yeon et al., 2005*), flow rate of 7.7 L.day^{-1} of CH$_4$ is possible, increasing the amount of

upgraded CH_4 by *c.* 44% in comparison with values obtained without CH_4 recovery. In this particular case, the incorporation of desorption and absorption membrane units into the UASB plant can be achieved relatively easily, in contrast to conventional desorption and absorption columns. Due to the limited space available and highest removal efficiencies obtained under low liquid flow rates, conventional equipment is not feasible.

5 Conclusions

5.1 Synthetic Mixtures

A poly-di-methyl-siloxane hollow fibre membrane contactor was applied for de-gassing of water saturated with pure CH_4 and binary CH_4:CO_2 mixture. The obtained results demonstrate that:

(i) Methane recovery is controlled by gas diffusivity within the membrane material; maximum methane recovery was recorded at lowest liquid velocity when utilising contactor with the thinnest wall.

(ii) Under optimum liquid hydrodynamic conditions a maximum de-gassing efficiency of 93% was achieved.

(iii) Methane recovery is dependent on the applied vacuum pressure; highest efficiencies were observed under the lowest vacuum pressure.

(iv) De-gassing of liquids is not governed by sweep gas velocity.

(v) Simultaneous recovery of carbon dioxide was possible; recovery of 88% was recorded under lowest liquid velocities. The presence of dissolved carbon dioxide has no effect on methane diffusion through the PDMS membrane.

5.2 Anaerobic Liquids

The potential for de-gassing low temperature anaerobic wastewater effluent has been demonstrated.

(i) On average, *c.* 45% of the produced methane is released in the dissolved form in the EGSB process effluent.

(ii) A maximum de-gassing efficiency of 72% with respect to dissolved methane was achieved.

(iii) On the gas side, low methane purity was observed and indicates that further work is required to facilitate efficient re-use.

(iv) Dissolved methane recovery could increase net energy production from low temperature anaerobic processes by *c.* +0.13 kWh m^{-3} and shift the net carbon footprint to net positive.

(v) The potential of integrating de-gassing contactor and membrane absorber into wastewater treatment flowsheet has been demonstrated; *c.* 44% greater methane flow rate in the upgraded biogas stream is possible with dissolved methane recovery.

(vi) Further experimental work is required to validate the long-term impact of biofouling on the process performance. In a future study, the employment of lumen feed mode could result in enhanced mass transfer. This option, however, will require the utilisation of a filter prior to liquid introduction into the fibre lumen in order to remove the larger suspended solids.

(vii) The subsequent economic analysis should encompass the following aspects: methane loss in the anaerobic effluent, downstream gas purity and its potential re-use, energy loss by the incorporation of a pump into the process, cost and lifetime of the PDMS module.

References

Alberto, M.C.R., Arah, J.R.M., Neue, H.U., Wassmann, R., Lantin, R.S., Aduna, J.B., Bronson, K.F. (2000) A sampling technoque for the determination of dissolved methane in soil solution. *Chemosphere: Global Change Science 2, 57-63.*

Al-Marzouqi, M., El-Naas, M., Marzouk, S., Abdullatif, N. (2008) Modeling of chemical absorption of CO_2 in membrane contactors. *Separation and Purification Technology 62, 499-506.*

Al-Saffar, H.B., Ozturk, B., Hughes, R. (1997) A comparison of porous and non-porous gas-liquid contactors for gas separation. *Transactions of the Institution of Chemical Engineering, 75, 685-692.*

Aptel, P., Semmens, M.J. (1996) Chapter 8: Multiphase membrane processes. In: Mallevialle, J.; Odendaal, P.E. and Wiesner, M.R. (eds.), Water Treatment – Membrane Processes, Mc Graw-Hill.

Atchariyawut, S., Feng, C., Wang, R., Jiraratananon, R. Liang, D.T. (2006) Effect of membrane structure on mass-transfer in the membrane gas-liquid contacting process using microporous PVDF hollow fibers. *Journal of Membrane Science 285, 272-281*.

Atchariyawut, S., Jiraratananon, R., Wang, R. (2007) Separation of CO_2 from CH_4 by using gas-liquid membrane contacting process. *Journal of Membrane Science 304, 163-172*.

Bandara, W.M.K.R.T., Ikeda, M., Satoh, H., Sasakawa, M., Nakahara, Y., Takahashi, M., Okabe, S. (2010) Recovery of dissolved methane gas discharged from a UASB reactor with a degassing membrane. In proceedings of the IWA World Water Congress. 20-23 September 2010, Montreal, Canada.

Barbe, A.M., Hogan, P.A., Johnson, R.A. (2000) Surface morphology changes during initial usage of hydrophobic, micro-porous polypropylene membranes. *Journal of Membrane Science 172, 197-216.*

Barbosa, R. A., Sant'Anna G. L. Jr. (1989) Treatment of raw domestic sewage in an UASB reactor. *Water Research 23, 1483-1490.*

Barzagli, F., Mani, F., Peruzzini, M. (2010) Continuous cycles of CO_2 absorption and amine regeneration with aqueous alkanolamines: a comparison of the efficiency between pure and blended DEA, MDEA and AMP solutions by ^{13}C NMR spectrometry. *Energy and Environmental Science 6, 772-779.*

Bhide. B.D., Voskericyan, A., Stern, S.A. (1998) Hybrid processes for the removal of acid gases from natural gas. *Journal of Membrane Science 140, 27-49.*

Bodzek, M. (2000) Membrane techniques in air cleaning. *Polish Journal of Environmental Studies 9, 1-12.*

Bos, A., Punt, I.G.M., Wessling, M., Strathmann, H. (1998) Plasticization-resistant glassy polyimide membranes for CO_2/CH_4 separations. *Separation and Purification Technology 14, 27-39.*

Bottino, A., Capannelli, G., Comite, A., Firpo, R., di Felice, R., Pinacci, P. (2006) Separation of carbon dioxide from flue gases using membrane contactors. *Desalination 200, 609-611.*

Boucif, N., Jefferson, B., Parsons, S.A., Judd, S.J., Stuetz, R.M. (2001) Direct molecular hydrogen sulphide scrubbing with hollow fibre membranes. In: *1st IWA International Conference on Odour and VOCs: measurement, regulation and control techniques: UNSW, 223-230.*

Bujalance, L., Wichern, M., Nettler, T., Paris, S., Bischof, F., Martinez, D., Horn, H. (2008) Increasing methane yield in municipal wastewater treatment at ambient temperature in a Vacuum Anaerobic Membrane Bioreactor (ANAMEM). In proceeding for the IWA Conference on Design and operation of

membrane plants for water, wastewater and industrial water. 1-2 October 2008, Amsterdam, The Netherlands.

Charati, S.G., Stern, S.A. (1998) Diffusion of gases in silicone polymers: molecular dynamics simulations. *Macromolecules 31, 5529-5535*.

Chen, H., Obuskovic, G., Majumdar, S., Sirkar, K.K. (2001) Immobilized glycerol-based liquid membranes in hollow fibers for selective CO_2 separation from CO_2-N_2 mixtures. *Journal of Membrane Science 183, 75-88*.

Chittrakarn, T., Bhongsuwan, T., Wanichapichart, P., Nuanuin, P., Chongkun, S., Bordeepong, S. (2002) Nuclear track-etched pore membrane production using neutrons from Thai research reactor TRR-1/M1. *Songklanakarin Journal of Science and Technology 24, 863-870*.

Cocchini, U., Nicolella, C., Livingston, A.G. (2002) Braided silicone rubber membranes for organic extraction from aqueous solutions - I. Mass transport studies. *Journal of Membrane Science 199, 85-99*.

Constant, M., Naveau, H., Ferrero, G.L., Nyns, E.J. (1989) Biogas end-use in the European community. *Elsevier Science Publisher, England*.

Costello, M.J., Fane, A.G., Hogan, P.A., Schofield, R.W. (1993) The effect of shell side hydrodynamics on the performance of axial flow hollow fibre modules. *Journal of Membrane Science 80, 1-11*.

CO_2 Capture Project (CCP) http://www.co2captureproject.org/index.htm (accessed 6 10 2013).

Crowder, R.O., Cussler, E.L. (1998) Mass transfer resistances in hollow fiber pervaporation. *Journal of Membrane Science 145, 173-184*.

Cussler, E.L. (1984) *Diffusion*, Cambridge University. Press, London.

Das, A., Abou-Nemah, I., Chandara, S., Sirkar, K.K. (1998) Membrane-moderated stripping process for removing VOCs from water in a composite hollow fiber module. *Journal of Membrane Science 148, 257-271*.

Department for environment food and rural affairs (DEFRA) (2007) Guidelines to Defra's GHG conversion factors for company reporting: Annexes updated June 2007 http://archive.defra.gov.uk/environment/business/reporting/pdf/conversion-factors.pdf (accessed 16 10 2010).

Dindore, V.Y., Brilman, D.W.F., Feron, P.H.M., Versteeg, G.F. (2004) CO_2 absorption at elevated pressures using hollow fiber membrane contactor. *Journal of Membrane Science 235, 99-109*.

Dindore, V.Y., Brilman, D.W.F., Geuzebroek, F.H., Versteeg, G.F. (2004) Membrane-solvent selection for CO_2 removal using membrane gas-liquid contactors. *Separation and Purification Technology 40, 133-145*.

Doig, S.D., Boam, A.T., Livingston, A.G., Stuckey, D.C. (1999) Mass transfer of hydrophobic solutes in solvent swollen silicone rubber membranes. *Journal of Membrane Science 154, 127-140*.

Feron, P.H.M., Jansen, A.E. (1999) Techno-economic analysis assessment of membrane gas absorption for the production of carbon dioxide from flue gas. In: Eliasson, B., Riemer, P., Wokaun, A. (eds), Greenhouse Gas Control Technologies, Pergamon, Oxford.

Ferreira, B.S., Fernandes, H.L., Reis, A., Mateus, M. (1998) Microporous hollow fibres for carbon dioxide absorption: Mass transfer model fitting and the supplying of carbon dioxide to microalgal cultures. *Journal of Chemical Technology and Biotechnology, 71, 60-70*.

Franco, J.A., deMontigny, D., Kentish, S.E., Perera, J.M., Stevens, G.W. (2009) Effect of amine degradation products on the membrane gas absorption process. *Chemical Engineering Science 64, 4016-4023*.

Gugliuzza, A., Drioli, E. (2007) PVDF and HYFON AD membranes: Ideal interfaces for contactor applications. *Journal of Membrane Science 300, 51-62*.

Hartley, K., Lant, P. (2006) Eliminating non-renewable CO_2 emissions from sewage treatment: an anaerobic migrating bed reactor pilot plant study. *Biotechnology and Bioengineering 95, 384-398*.

Herzog, H.J. (2001) What future for carbon capture and sequestration. *Environmental Science and Technology 35, 148-153*.

Hoff, K.A., Svendsen, H.F. (2013) CO_2 absorption with membrane contactors vs. packed absorbers – Challenges and opportunities in post combustion capture and natural gas sweetening. *Energy Procedia 37, 952-960*.

Husain, S., Koros, W. (2007) Mixed matrix hollow fiber membranes made with modified HSSZ-13 zeolite in polyetherimide polymer matrix for gas separation. *Journal of Membrane Science 288, 195-207*.

IEA Bioenergy, http://www.biogasmax.org/media/iea_2biogas_upgrading_tech__025919000_1434_30032010.pdf (accessed 06 12 2010).

IPCC Fourth Assessment Report: Climate Change 2007, http://www.ipcc.ch/publications_and_data/ar4/wg1/en/ch2s2-10-2.html (accessed 02 12 2010).

Isamil, A.F., Yaacob, N. (2006) Performance of treated and untreated asymmetric polysulfone hollow fiber membrane in series and cascade module configurations for CO_2/CH_4 gas separation system. *Journal of Membrane Science 275, 151-165*.

Ito, A., Yamagiwa, K., Tamura, M., Furusawa, M. (1998) Removal of dissolved oxygen using non-porous hollow-fiber membranes. *Journal of Membrane Science 145, 111-117*.

Keshavarz, P. Fathikalajahi, J., Ayatollahi, S. (2008) Analysis of CO_2 separation and simulation of a partially wetted hollow fiber membrane contactor. *Journal of Hazardous Materials 152, 1237-1247*.

Keshavarz, P., Fathikalajahi, J., Ayatollahi, S. (2008) Mathematical modelling of the simultaneous absorption of carbon dioxide and hydrogen sulfide in a hollow fiber membrane contactor. *Separation and Purification Technology 63, 145-155*.

Khaisri, S., deMontigny, D., Tontiwachwuthikul, P., Jiraratanon, R. (2009) Comparing membrane resistance and absorption performance of three different membranes in a gas absorption membrane contactor. *Separation and Purification Technology 65, 290–297*.

Kim, H., Kim, D., Yang, J.S., Kim, C. (2006) Sample preparation for headspace GC analysis of residual solvents in hyaluronic acid derivative fiber. *Bulletin of the Korean Chemical Society 27, 302-304*.

Klaassen, R., Jansen, A.E. (2001) The membrane contactor: Environmental applications and possibilities. *Environmental Progress 20, 37-43*.

Ko, J.-J., Li, M.-H. (2000) Kinetics of absorption of carbon dioxide into solutions of N-methyldiethanolamine + water. *Chemical Engineering Science 55, 4139-4147*.

Kobayashi, H.A., Stenstrom, M.K., Mah, R.A. (1983) Treatment of low strength domestic wastewater using the anaerobic filter. *Water Research 17, 903-909*.

Kohl, A.L., Nielsen, R.B. (1997) Gas purification. 5th Edition, Gulf Publishing Co., Houston, Texas.

Kosaraju, P., Kovvali, A.S., Korikov, A., Sirkar, K.K. (2005) Hollow fiber membrane contactors based CO_2 absorption-stripping using novel solvents and membranes. *Industrial and Engineering Chemistry Research 44, 1250-1258*.

Kreulen, H. (1993). Microporous membranes in gas separation processes using a liquid phase. PhD thesis, University of Twente. The Netherlands.

Kumar, P.S., Hogendoorn, J.A., Feron, P.H.M., Versteeg, G.F. (2002) New absorption liquids for the removal of CO_2 from dilute gas streams using membrane contactors. *Chemical Engineering Science 57, 1639-1651*.

Lettinga, G., Roersma, R., Grin, P. (1983) Anaerobic treatment of raw domestic sewage at ambient temperatures using a granular bed UASB reactor. *Biotechnology and Bioengineering 25, 1701-1723*.

Leveque, M.A. (1928) Les lois de transmission de chaleur par convection. *Annales des Mines 13, 201-299*.

Li, K., Teo, W.K. (1998) Use of permeation and absorption methods for CO_2 removal in hollow fibre membrane modules. *Separation and Purification Technology 13, 79-88*.

Lin, S.-H., Chiang, P.-C., Hsieh, C.-F., Li, M.-H., Tung, K.L. (2008) Absorption of carbon dioxide by the absorbent composed of piperazine and 2-amino-2-methyl-1-propanol. *Journal of the Chinese Institute of Chemical Engineers 39, 13-21*.

Lin, S.-H., Tung, K-L., Chang, H.-W., Lee, K.-R. (2009) Influence of fluorocarbon flat-membrane hydrophobicity on carbon dioxide recovery. *Chemosphere 75, 1410-1416*.

Lu, J.-G., Zheng, Y.-F., Cheng, M.-D. (2008) Wetting mechanism in mass transfer process of hydrophobic membrane gas absorption. *Journal of Membrane Science 308, 180-190*.

Lu, J.-G., Zheng, Y.-F., Cheng, M.-D., Wang, L.-J. (2007) Effect of activators on mass-transfer enhancement in a hollow fiber contactor using activated alkanolamine solutions. *Journal of Membrane Science 308, 138-149*.

94

Matson, S.L., Lopez, J., Quinn, J.A. (1983) Separation of gases with synthetic membranes. *Chemical Engineering Science 38, 503-524.*

Mavroudi, M., Kaldis, S.P., Sakellaropoulos, G.P. (2003) Reduction of CO_2 emissions by a membrane contacting process. *Fuel 82, 2153-2159.*

Mavroudi, M., Kaldis, S.P., Sakellaropoulos, G.P. (2006) A study of mass transfer resistance in membrane gas-liquid contacting process. *Journal of Membrane Science 272, 103-115.*

McAdam, E.J., Judd, S.J. (2008) Optimisation of dead-end filtration conditions for an immersed anoxic membrane bioreactor. *Journal of Membrane Science 325, 940-946.*

McAdam, E.J., Lüffler, D., Martin-Garcia, N., Eusebi, A.L., Lester, J.N., Jefferson, B., Cartmell, E. (2010) Integrating anaerobic processes into wastewater treatment. In proceedings of the 7th IWA Leading-Edge Conference on Water and Wastewater Technologies, Phoenix, Arizona, 2-4 June, 2010.

Merkel, T.C., Nagai, V.I., Freeman, B.D., Pinnau, I. (2000) Gas sorption, difussion and permeation in poly(dimethylsiloxane). *Journal of Polymer Science: Part B: Polymer Physics 38, 415-434.*

National Grid
http://www.nationalgrid.com/uk/Gas/Data/help/opdata/index.htm (accessed 06 12 2010).

Nicholas, G.R., Harris, P.R. (1997) Power generation from a large covered Lagoon. *Water 24, 19.*

Noyola, A., Capdeville, B., Roques, H. (1988) Anaerobic treatment of domestic sewage with a rotating-stationary fixed-film reactor. *Water Research 22, 1585-1592.*

Pinnau, I., He, Z. (2004) Pure- and mixed-gas permeation properties of Polydimethylsiloxane for hydrocarbon/methane and hydrocarbon/hydrogen separation. *Journal of Membrane Science 244, 227-233*.

Poddar, T.K., Majumdar, S., Sirkar, K.K. (1996) Removal of VOCs from air by membrane-based absorption and stripping. *Journal of Membrane Science 120, 221-237*.

Porcheron, F., Drozdz, S. (2009) Hollow fiber membrane contactor transient experiments for the characterization of gas/liquid thermodynamics and mass transfer properties. *Chemical Engineering Science 64, 265-275*.

Raharjo, R.D., Freeman, B.D., Paul, D.R., Sarti G.C., Sandres, E.S. (2007) Pure and mixed gas CH_4 and $n-C_4H_{10}$ permeability and diffusivity in poly(dimethylsiloxane). *Journal of Membrane Science 306, 75-92*.

Rangwala, H.A. (1996) Absorption of carbon dioxide into aqueous solutions using hollow fiber membrane contactors. *Journal of Membrane Science 112, 229-240*.

Robb, W.L. (1986) Thin silicone membranes – their permeation properties and some applications. *Annals New York Academy of Sciences 146, 119-137*.

Rongwong, W., Jiraratananon, R., Atchariyawut, S. (2009) Experimental study on membrane wetting in gas-liquid membrane contacting process for CO_2 absorption by single and mixed absorbents. *Separation and Purification Technology 69, 118-125*.

Sadrzadeh, M., Amirilargani, K.S., Shahidi, K., Mohammadi, T. (2009) Gas permeartion through a synthesised composite PDMS/PES membranes. *Journal of Membrane Science 342, 236-250*.

Sea, B., Park, Y.-I., Lee, K.-H. (2002) Comparison of porous hollow fibres as a membrane contactor for carbon dioxide absorption. *Journal of Industrial and Engineering Chemistry 3, 290-296*.

Seekkuarachchi, I.N., Komami, J., Kumazawa, H. (2008) Augmentation of absorption and desorption rates in a hydrophobic microporous hollow fiber contained contactor by adjusting outlet gas pressure. *Chemical Engineering Communications 195, 57-71.*

Simons, K., Nijmeijer, K., Wessling, M. (2009) Gas-liquid membrane contactors for CO_2 removal. *Journal of Membrane Science 340, 214-220.*

Singh, K. S., Harada, H., Viraraghavan, T. (1996) Low-strength wastewater treatment by a UASB reactor. *Bioresource Technology 55, 187-194.*

Smith A.R., Klosek, J. (2001) A review of air separation technologies and their integration with energy conversion processes. *Fuel Processing Technology 70, 115-134.*

Stajonevic, M., Lazarevic, M., Radic, D. (2003) Review ofmembrane contactors design and applications of different modules in industry. *Faculty of Mechanical Engineering Transactions 31, 91-98.*

Stern, S.A. (1994) Polymers for gas separation: the next decade. *Journal of Membrane Science 94, 1-65.*

Strazisar, B.R., Anderson, R.R., White, C.M. (2003) Degradation pathways for monoethanolamine in a CO_2 capture facility. *Energy and Fuels, 17, 1034-1039.*

Sun, W.-C., Yong, C.-B., Li, M.-H. (2005) Kinetics of the absorption of carbon dioxide into mixed aqueous solutions of 2-amino-2-methyl-1-propanol and piperazine. *Chemical Engineering Science 60, 503-516.*

Tamai, Y. (1994) Molecular simulation of permeation of small penetrants through membranes. 1. Diffusion coefficients. *Macromolecules 27, 4498-4508.*

Tan, X., Capar, G., Li, K. (2005) Analysis of dissolved oxygen removal in hollow fibre membrane modules: effect of water vapour. *Journal of Membrane Science 251, 111-119.*

Tchobanoglous, G., Burton, L.F., Stensel, H.D. (2003) Wastewater Engineering Treatment and Reuse 4th Edition. Metcalf and Eddy McGraw-Hill Companies, Inc. US.

Tremblay, P., Savard, M.M., Vermette, J., Paquin, R. (2006) Gas permeability, diffusivity and solubility of nitrogen, helium, methane, carbon dioxide and formaldehyde in dense polymeric membranes using a new on-line permeation apparatus. *Journal of Membrane Science 282, 245-256*.

Uemura, S., Harada, H. (2000) Treatment of sewage by a UASB reactor under moderate to low temperature conditions. *Bioresource Technology 72, 275-282*.

Vallieres, C., Favre, E. (2004) Vacuum versus sweeping gas operation for binary mixtures separation by dense membrane processes. *Journal of Membrane Science 244, 17-23*.

Van Landeghem, H. (1980) Multiphase reactors: mass transfer and modelling. *Chemical Engineering Science 35, 1912-1949*.

Walsh, K.P., McLaughlan, R.G. (1999) Bubble extraction of dissolved gases from groundwater samples. *Water, Air and Soil Pollution 115, 525-534*.

Wang, R., Li, D.F., Zhou, C., Liu, M., Liang, D.T (2004) Impact of DEA solutions with and without CO_2 loading on porous polypropylene membranes intended for use as contactors. *Journal of Membrane Science 229,147-157*.

Wang, R., Zhang, H.Y., Feron, P.H.M., Liang, D.T. (2005) Influence of membrane wetting on CO_2 capture in microporous hollow fiber membrane contactors. *Separation and Purification Technology 46, 22-40*.

Weiss, R.F. (1974) Carbon dioxide in water and seawater: the solubility of a non-ideal gas. *Marine Chemistry 2, 203-215*.

Wilson, E.E. (1915) A basis for rational design of heat transfer apparatus. *Transactions of the American Society of Mechanical Engineers 37, 47-71*.

Xu, J.B., Lange, S., Bartley, J.P., Johnson, R.A. (2004) Alginate-coated microporous PTFE membranes for use in the osmotic distillation of oily feeds. *Journal of Membrane Science 240, 81-89*.

Xu, S., Wang, Y.W., Otto, F.D., Mather, A.E. (1996) Kinetics of the reaction of carbon dioxide with 2-amino-2-methyl-1-propanol solutions. *Chemical Engineering Science 51, 841-850*.

Yamamoto, S., Alcauskas, J.B., Crozier, T.E. (1976) Solubility of methane in distilled water and seawater. *Journal of Chemical and Engineering Data 21, 78-80*.

Yan, S., Fang, M., Zhang, W., Zhong, W., Luo, Z., Cen, K. (2008) Comparative analysis of CO_2 separation from flue gas by membrane gas absorption technology and chemical absorption in China. *Energy Conversion and Management 49, 3188-3197*.

Yang, M.C., Cussler, E.L. (1986) Designing hollow fiber contactors. *American Institute of Chemical Engineers Journal 32, 1910-1916*.

Yang, Q., Xu, Z.-K., Dai, Z.-W., Wang, J.L., Ulbricht, M. (2005) Surface modification of polypropylene microporous membranes with a novel glycopolymer. *Chemistry of Materials, 17, 3050-3058*.

Yeon, S.-H, Lee, K.-S., Sea, B., Park, Y.-I., Lee, K.-H. (2005) Application of pilot-scale membrane contactor hybrid system for removal of carbon dioxide from flue gas. *Journal of Membrane Science 257, 156-160*.

Zhang, H., Wang, R., Liang, D.T., Tay, J.H. (2008) Theoretical and experimental studies of membrane wetting in the membrane gas-liquid contacting process for CO_2 absorption. *Journal of Membrane Science 308, 162-17*.